CAMBRIDGE
UNIVERSITY PRESS

RESEARCH ARTICLE

Integrated sliding mode control with input restriction, output feedback and repetitive learning for space robot with flexible-base, flexible-link and flexible-joint

Xiaodong Fu[1,2], Haiping Ai[1,2,*] (ID) and Li Chen[2]

[1]School of Energy and Mechanical Engineering, Jiangxi University of Science and Technology, Nanchang, 330013 Jiangxi, China and [2]School of Mechanical Engineering and Automation, Fuzhou University, Fuzhou, 350108 Fujian, China
*Corresponding author. E-mail: ahpwuhan@163.com

Abstract

In the control of space robots, flexible vibrations exist in the base, links and joints. When building a motion control scheme, the following three aspects should be considered: (1) the complexity in dynamic modeling; (2) the low accuracy of motion control and (3) the simultaneous suppression of multiple flexible vibrations. In this paper, we propose a motion vibration integrated saturation control scheme. First, the dynamic model of space robot with flexible-base, flexible-link and flexible-joint is established according to the assumed modes method and Lagrange equation. Second, singular perturbation theory is used to decompose the model into two subsystems: a slow subsystem containing the rigid motions of base and joints as well as the vibration of links, and a fast subsystem containing vibrations of base and joints. Third, an integrated sliding mode control with input restriction, output feedback and repetitive learning (ISMC-IOR) is designed, which can track the desired trajectories of base and joints with -3 orders of magnitude accuracy, while suppressing the multiple flexible vibrations of base, links and joints 50%–80% and 37% performance improvement over ISMC-IOR-NV were achieved. Finally, the algorithm is verified by simulations.

1. Introduction

Space robots are systems with a certain topology that are articulated by multiple connecting links. They are widely used in space operations [1, 2] and play an important role in the construction process of the space station [3]. In recent years, with the increasing demand for space manipulation accuracy, high-precision control of space robots draws attention [4, 5]. As non-negligible factors affecting control accuracy, the topic of flexibilities in the base, link and joint on space robot becomes an important subject. The links of space robot are generally designed to be thin and long, which is prone to vibration when performing tasks, especially auxiliary docking or capture operations [6]. Space robot with movable link on the base is more maneuverable and with larger working range, compared to one with fixed link. However, the movable link is mounted on the slender base truss rail; thus, it is easily affected by external shocks such as drive torque or cosmic rays, leading to base vibration. In addition, space robot links are generally driven by lightweight harmonic flexible wheels mounted at the joints, gaining the advantages of being small size, light-weighted and with large transmission ratio at the price of out-of-sync problem between the space robot motor and the joint, resulting in joint vibration [7]. These flexible vibrations, once excited, can take a very long time to decay in the undamped space environment. In order to reduce the influence of the structural flexibility of the system, a "low-speed, slow-running" operation model is commonly used, but this operation model is time-consuming and laborious. Therefore, it is of great

practical importance to study the influence of the flexibility of base, link and joint in the mathematical modeling and controller design for space robots.

For space robots with flexible base, links and joints, the non-completeness of dynamics and the strong coupling between rigid and flexible motions greatly increase the difficulty in dynamics analyzing and controller designing. Most researches on space robot address the flexibility problem by focusing on either the link [8] or the joint [9], while studies on base flexibility are mostly found in ground robot systems [10, 11]. Mori *et al.* [12] presented an impedance and vibration suppression fusion control for a flexible-base manipulator, but it was not suitable for space weightlessness environment nor did it consider the effect of link flexibility. Yu [13] analyzed a flexible-link space robot considering the influence of base flexibility on system modeling and control, but the experimental implementation process of the flexible-link is not presented. Designing actual flexible arms is very important in fast and high-precision control situations and has received a lot of attention from scholars [14, 15]. Aghajari *et al.* [16] proposed a kind of flexible-link that can achieve fast movements and precise positioning and has a wide range of applications in the field of space exploration. Zhang *et al.* [17] studied the dynamics and control of a flexible-link space robot considering friction and joint flexibility. A trajectory tracking controller with friction compensation was designed, but base flexibility was not included. Xie *et al.* [18] proposed a dynamics model considering the flexibility in links and joints and used fuzzy sliding mode control to achieve joint trajectory tracking. For the fast subsystem, a velocity difference feedback control and a linear quadratic optimal control were designed to suppress the vibration of the flexible links and joints, respectively. Although the expected results were achieved, the fast subsystem vibration suppression algorithm composed of two algorithms was with complex structure and required large computational efforts. To the best of our knowledge, it is still an open topic to combine the three aspects (i.e. flexibilities of base, link and joint) regarding model building and controller designing. In order to improve the aerospace performance of flexible-base, flexible-link and flexible-joint (FBFLFJ) space robot in extreme environments, it is particularly important to control the motion vibration synchronization.

Space robots are costly from software and hardware development, especially in control algorithm design. The good controllers contribute to cost-saving and efficiency in practice [19, 20]. The followings are three aspects to be considered. First, the power and torque of the drive motor are always limited on space robots; therefore, the input constraints should be considered to avoid control failure [21, 22]. Second, output feedback based on position sensing is preferred when speed sensors are not available [23]. Third, repetitive learning control can be introduced to accommodate reoccurring errors in periodic tasks [24, 25]. Liu *et al.* [26] proposed a control strategy for momentum constraint under external disturbances and input saturation. Zhang *et al.* [27] proposed an output feedback predictive control strategy to achieve coordination and synchronous stabilization with output consistency. Califano *et al.* [28] proposed exponentially stable repetitive learning algorithms and gave an explicit proof of fully localized asymptotic tracking and interference suppression. The abovementioned control algorithms are mainly designed for single working conditions, while in practice, the controller must take on all the three aspects.

Based on the above considerations, this paper establishes an FBFLFJ space robot dynamics model using the hypothetical modal method with Lagrange's equation and decomposes the model according to the principle of mutual independence of dual time scales by using the singular perturbation method. Due to the three flexibilities being coupled with each other, it is very difficult to suppress the vibration at the same time. In this paper, the vibration of base and joint is decomposed in fast subsystem, and the vibration of link is decomposed in slow subsystem. Then, the vibrations of base and joint are suppressed with linear quadratic optimal controller, and the vibration of the link is suppressed by hybrid trajectory method based on the virtual force concept. Finally, considering the restricted drive torque, unmeasurable velocity information and uncertain model information of space robot, we propose an integrated sliding mode control with input restriction, output feedback and repetitive learning (ISMC-IOR). By using the class invariance theorem, the stability of the algorithm is proved, and the simulation analysis is performed to verify its effectiveness.

The rest of the paper is organized as follows: in Section 2, an FBFLFJ space robot is introduced, and its dynamic model is developed using the assumed mode method and Lagrange method. In Section 3,
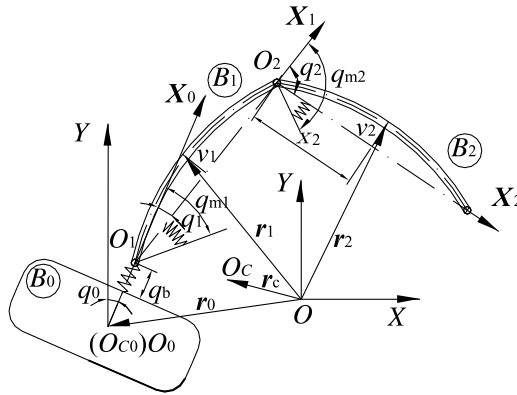
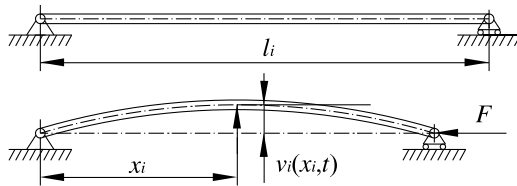**Figure 1.** *Structure diagram of the FBFLFJ space robot system.*

Figure 2. *Structure diagram of the flexible link.*

the FBFLFJ space robot is decomposed into fast and slow subsystems using the singular perturbation method, and its properties are introduced. In Section 4, the motion and vibration integrated control method is presented and its stability is investigated. In Section 5, experimental data from a computer simulation are presented. Section 6 gives the conclusion.

2. Dynamic model of an FBFLFJ space robot

The flexible-base flexible-link and flexible-joint (FBFLFJ) space robot system is shown in Figure 1. It consists of a free-floating flexible-base B_0, and flexible-link B_1 and flexible-link B_2. The inertial coordinate system OXY and the local coordinate systems $O_{i'}X_{i'}Y_{i'}(i' = 0, 1, 2)$ of each split are established. O_0 coincides with the base mass center O_{C0}, and O_i coincides with the joint hinge center connecting the split B_{i-1} and B_i $(i = 1, 2)$. q_b is the flexible deformation of the base, q_0 is the base attitude angle, q_i is the relative angle of the link B_i and q_{mi} is the joint motor rotor angle $(i = 1, 2)$. When the base is not deformed, the distance between O_{C0} and O_1 is l_0. The mass of the base is m_0, and the rotational inertia is J_0. The initial length of link B_i is l_i, the density is ρ_i and the motor rotor rotational inertia is $J_{mi}(i = 1, 2)$.

According to the configuration and vibration characteristics of the FBFLFJ robot links, each link is simplified to a simply supported beam, as shown in Fig. 2, and analyzed by Euler-Bernoulli beam theory and hypothetical modal method. Taking its flexural stiffness EI_i as a constant value, the flexible deformation of the link B_i at x_i section at the moment t is $v_i(x_i, t) = \sum_{j=1}^{n_i} \phi_{ij}(x_i) \, \delta_{ij}(t)$, $(0 \leq x_i \leq l_i)$, where x_i is any distance on the coordinate system X_i of the main axis of link B_i, ϕ_{ij} and δ_{ij} represent the j-order modal function and corresponding modal coordinates of link B_i, respectively. Taking the retained modal number as $n_i = 2$, the equivalent stiffness factor of link B_i is $k_{\delta ij} = EI_i \int_0^{l_i} \left(\ddot{\phi}_{ij}^2(x_i) \right) dx_i$, $(i, j = 1, 2)$.

According to the SPONG assumption [29], the flexible base and the flexible joints are assumed to be massless linear telescopic spring and linear torsional spring, respectively. The elasticity coefficients of base and joint are defined as k_b and $k_{mi}(i = 1, 2)$, respectively, and are taken as constant values. The flexible-joint structure is shown in Fig. 3.
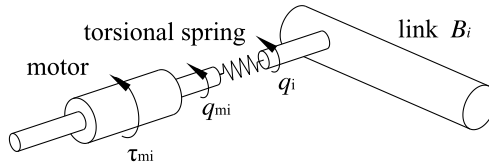
Figure 3. *Structure diagram of the flexible joint.*

According to the geometric position relationship of the FBFLFJ space robot in the inertial coordinate system, we have

$$
\begin{cases}
\boldsymbol{r}_0 = (x_0, y_0)^T \\
\boldsymbol{r}_1 = \boldsymbol{r}_0 + (l_0 + q_b)\,\boldsymbol{e}_0 + x_1\boldsymbol{e}_1 + v_1(x_1, t)\,\boldsymbol{c}_1 \\
\boldsymbol{r}_2 = \boldsymbol{r}_0 + (l_0 + q_b)\,\boldsymbol{e}_0 + l_1\boldsymbol{e}_1 + x_2\boldsymbol{e}_2 + v_2(x_2, t)\,\boldsymbol{c}_2
\end{cases}
\tag{1}
$$

where $\boldsymbol{r}_0$ denotes the position vector of the base mass center in the inertial coordinate system, and $\boldsymbol{r}_i$ denotes the vector of any point on the link B_i in the inertial coordinate system $(i = 1, 2)$. (x_0, y_0) is the base center of mass coordinate. $\boldsymbol{e}_0 = \begin{bmatrix} \sin(q_0) \\ \cos(q_0) \end{bmatrix}$, $\boldsymbol{e}_1 = \begin{bmatrix} \sin(q_0 + q_1) \\ \cos(q_0 + q_1) \end{bmatrix}$, $\boldsymbol{c}_1 = \begin{bmatrix} -\cos(q_0 + q_1) \\ \sin(q_0 + q_1) \end{bmatrix}$, $\boldsymbol{e}_2 = \begin{bmatrix} \sin(q_0 + q_1 + q_2) \\ \cos(q_0 + q_1 + q_2) \end{bmatrix}$ and $\boldsymbol{c}_2 = \begin{bmatrix} -\cos(q_0 + q_1 + q_2) \\ \sin(q_0 + q_1 + q_2) \end{bmatrix}$ are the basis vectors.

According to the centroid theorem, we have

$$
m_0\boldsymbol{r}_0 + \sum_{i=1}^{2} \int_0^{l_i} \rho_i \boldsymbol{r}_i \mathrm{d}x_i = M\boldsymbol{r}_C,
\tag{2}
$$

where $\boldsymbol{r}_C$ denotes the position vector of the total center of mass of the system in the inertial coordinate system, and the total mass of the system is $M = m_0 + \sum_{i=1}^{2} \rho_i l_i$.

Let the initial momentum of the system be 0, then $M\dot{\boldsymbol{r}}_C = 0$. Combining Eqs. (1) and (2), the total kinetic energy of the FBFLFJ space robot system can be obtained as

$$
T = \frac{1}{2}m_0\dot{\boldsymbol{r}}_0^2 + \frac{1}{2}J_0\dot{q}_0^2 + \sum_{i=1}^{2}\left(\frac{1}{2}\int_0^{l_i}\rho_i\dot{\boldsymbol{r}}_i^2\mathrm{d}x_i\right) + \sum_{i=1}^{2}\left(\frac{1}{2}J_{mi}\dot{q}_{mi}^2\right).
\tag{3}
$$

Neglecting the effect of gravity, the total potential energy of the FBFJFL space robot system is

$$
V = \frac{1}{2}k_b q_b^2 + \sum_{i=1}^{2}\left(\frac{\mathrm{EI}_i}{2}\int_0^{l_i}\left(\frac{\partial^2 v_i(x_i, t)}{\partial x_i^2}\right)^2 \mathrm{d}x_i\right) + \sum_{i=1}^{2}\left(\frac{1}{2}k_{mi}(q_{mi} - q_i)^2\right).
\tag{4}
$$

Let $L = T - V$ be the Lagrange function, and substitute Eqs. (3) and (4) into the Lagrange equation to obtain the FBFLFJ space robot dynamics model with uncontrolled base position and controlled attitude, as

$$
\begin{bmatrix} \boldsymbol{D}(\boldsymbol{q}_{boj\delta}) & \boldsymbol{0} \\ \boldsymbol{0} & \boldsymbol{J}_m \end{bmatrix}\begin{bmatrix} \ddot{\boldsymbol{q}}_{boj\delta} \\ \ddot{\boldsymbol{q}}_m \end{bmatrix} + \begin{bmatrix} \boldsymbol{H}(\boldsymbol{q}_{boj\delta}, \dot{\boldsymbol{q}}_{boj\delta}) & \boldsymbol{0} \\ \boldsymbol{0} & \boldsymbol{0} \end{bmatrix}\begin{bmatrix} \dot{\boldsymbol{q}}_{boj\delta} \\ \dot{\boldsymbol{q}}_m \end{bmatrix} + \begin{bmatrix} \boldsymbol{\xi}_{boj\delta} \\ \boldsymbol{K}_m\boldsymbol{\sigma} \end{bmatrix} = \begin{bmatrix} \boldsymbol{\tau}_{boj\delta} \\ \boldsymbol{\tau}_m \end{bmatrix},
\tag{5}
$$

where $\boldsymbol{D}(\boldsymbol{q}_{boj\delta})$ is the symmetric positive definite mass matrix, and $\boldsymbol{H}(\boldsymbol{q}_{boj\delta}, \dot{\boldsymbol{q}}_{boj\delta})$ denotes the centrifugal force matrix. Here $\boldsymbol{q}_{boj\delta} = \begin{bmatrix} q_b & \boldsymbol{q}_{oj\delta}^T \end{bmatrix}^T$, $\boldsymbol{q}_{oj\delta} = \begin{bmatrix} \boldsymbol{q}^T & \boldsymbol{\delta}^T \end{bmatrix}^T$, $\boldsymbol{q} = \begin{bmatrix} q_0 & \boldsymbol{q}_j^T \end{bmatrix}^T$, $\boldsymbol{q}_j = \begin{bmatrix} q_1 & q_2 \end{bmatrix}^T$, $\boldsymbol{\delta} = \begin{bmatrix} \delta_{11} & \delta_{12} & \delta_{21} & \delta_{22} \end{bmatrix}^T$, $\boldsymbol{q}_m = \begin{bmatrix} q_{m1} & q_{m2} \end{bmatrix}^T$, $\boldsymbol{J}_m = \mathrm{diag}(J_{m1}, J_{m2})$, $\boldsymbol{K}_\delta = \mathrm{diag}(k_{\delta11}, k_{\delta12}, k_{\delta21}, k_{\delta22})$, $\boldsymbol{K}_m = \mathrm{diag}(k_{m1}, k_{m2})$, $\boldsymbol{\sigma} = \boldsymbol{q}_m - \boldsymbol{q}_j$, $\boldsymbol{\xi}_{boj\delta} = \begin{bmatrix} k_b q_b & 0 & -(\boldsymbol{\tau})^T & (\boldsymbol{K}_\delta\boldsymbol{\delta})^T \end{bmatrix}^T$, $\boldsymbol{\tau}_{boj\delta} = \begin{bmatrix} 0 & \tau_0 & \boldsymbol{0}^T \end{bmatrix}^T$. $\boldsymbol{\tau}_m = \begin{bmatrix} \tau_{m1} & \tau_{m2} \end{bmatrix}^T$ is the motor rotor control torque.

3. Model decomposition and properties of the FBFLFJ space robot

3.1. FBFLFJ space robot model singular perturbation decomposition

To facilitate the control analysis of the FBFLFJ space robot, the model is firstly decomposed and Eq. (5) is rewritten as

$$\boldsymbol{D}(\boldsymbol{q}_{boj\delta})\ddot{\boldsymbol{q}}_{boj\delta} + \boldsymbol{H}(\boldsymbol{q}_{boj\delta}, \dot{\boldsymbol{q}}_{boj\delta})\dot{\boldsymbol{q}}_{boj\delta} + \boldsymbol{\xi}_{boj\delta} = \boldsymbol{\tau}_{boj\delta}, \tag{6}$$

$$\boldsymbol{J}_m\ddot{\boldsymbol{q}}_m + \boldsymbol{\tau} = \boldsymbol{\tau}_m, \tag{7}$$

$$\boldsymbol{\tau} = \boldsymbol{K}_m\boldsymbol{\sigma}. \tag{8}$$

Rewrite the matrices $\boldsymbol{D}(\boldsymbol{q}_{boj\delta})$ and $\boldsymbol{H}(\boldsymbol{q}_{boj\delta}, \dot{\boldsymbol{q}}_{boj\delta})$ from Eq. (6) as $\begin{bmatrix} \boldsymbol{D}_{aa} & \boldsymbol{D}_{ab} \\ \boldsymbol{D}_{ba} & \boldsymbol{D}_{bb} \end{bmatrix}$ and $\begin{bmatrix} \boldsymbol{H}_{aa} & \boldsymbol{H}_{ab} \\ \boldsymbol{H}_{ba} & \boldsymbol{H}_{bb} \end{bmatrix}$, respectively, in which $\boldsymbol{D}_{aa}, \boldsymbol{H}_{aa} \in \mathbb{R}^{1\times 1}, \boldsymbol{D}_{ab}, \boldsymbol{H}_{ab} \in \mathbb{R}^{1\times 7}, \boldsymbol{D}_{ba}, \boldsymbol{H}_{ba} \in \mathbb{R}^{7\times 1}, \boldsymbol{D}_{bb}, \boldsymbol{H}_{bb} \in \mathbb{R}^{7\times 7}$. $\boldsymbol{D}(\boldsymbol{q}_{boj\delta})$ is invertible and can be defined by

$$\begin{bmatrix} \boldsymbol{N}_{11} & \boldsymbol{N}_{12} \\ \boldsymbol{N}_{21} & \boldsymbol{N}_{22} \end{bmatrix} = \begin{bmatrix} \boldsymbol{D}_{aa} & \boldsymbol{D}_{ab} \\ \boldsymbol{D}_{ba} & \boldsymbol{D}_{bb} \end{bmatrix}^{-1}, \tag{9}$$

where $\boldsymbol{N}_{11} \in \mathbb{R}^{1\times 1}, \boldsymbol{N}_{12} \in \mathbb{R}^{1\times 7}, \boldsymbol{N}_{21} \in \mathbb{R}^{7\times 1}$ and $\boldsymbol{N}_{22} \in \mathbb{R}^{7\times 7}$.

By substituting Eq. (9) into Eq. (6), we obtain

$$\ddot{q}_b = -\boldsymbol{N}_{11}\big(\boldsymbol{H}_{aa}\dot{q}_b + \boldsymbol{H}_{ab}\dot{\boldsymbol{q}}_{oj\delta} + k_bq_b\big) - \boldsymbol{N}_{12}\big(\boldsymbol{H}_{ba}\dot{q}_b + \boldsymbol{H}_{bb}\dot{\boldsymbol{q}}_{oj\delta}\big) + \boldsymbol{N}_{12}\begin{bmatrix} \tau_0 \\ \boldsymbol{\tau} \\ -\boldsymbol{K}_\delta\boldsymbol{\delta} \end{bmatrix}, \tag{10}$$

$$\ddot{\boldsymbol{q}}_{oj\delta} = -\boldsymbol{N}_{21}\big(\boldsymbol{H}_{aa}\dot{q}_b + \boldsymbol{H}_{ab}\dot{\boldsymbol{q}}_{oj\delta} + k_bq_b\big) - \boldsymbol{N}_{22}\big(\boldsymbol{H}_{ba}\dot{q}_b + \boldsymbol{H}_{bb}\dot{\boldsymbol{q}}_{oj\delta}\big) + \boldsymbol{N}_{22}\begin{bmatrix} \tau_0 \\ \boldsymbol{\tau} \\ -\boldsymbol{K}_\delta\boldsymbol{\delta} \end{bmatrix}. \tag{11}$$

Now the singular perturbation decomposition is performed for the system: treat $\boldsymbol{q}_{oj\delta}$ as slow sub-variable, and treat q_b and $\boldsymbol{\sigma}$ as fast sub-variables. $\mu = 1/\min(k_b, k_{m1}, k_{m2})$ is defined as the singular perturbation factor, and $t_f = t/\sqrt{\mu}$ is the fast time scale, where the equivalent stiffness coefficients of the base and the joints at this time scale are k_{bf} and $\boldsymbol{K}_{mf}$, respectively, and the flexible deformations are q_{bf} and $\boldsymbol{\sigma}_f$, respectively, where $k_{bf} = \mu k_b, \boldsymbol{K}_{mf} = \mu\boldsymbol{K}_m, q_{bf} = q_b/\mu$, and $\boldsymbol{\sigma}_f = \boldsymbol{\sigma}/\mu$. The following relation exists

$$k_bq_b = \frac{k_{bf}}{\mu}q_{bf}\mu = k_{bf}q_{bf}, \tag{12}$$

$$\boldsymbol{K}_m\boldsymbol{\sigma} = \frac{\boldsymbol{K}_{mf}}{\mu}\boldsymbol{\sigma}_f\mu = \boldsymbol{K}_{mf}\boldsymbol{\sigma}_f. \tag{13}$$

By substituting $q_{bf} = q_b/\mu$, Eqs. (12) and (13) into Eqs. (10) and (11), we get

$$\mu\ddot{q}_{bf} = -\boldsymbol{N}_{11}\big(\boldsymbol{H}_{aa}\mu\dot{q}_{bf} + \boldsymbol{H}_{ab}\dot{\boldsymbol{q}}_{oj\delta} + k_{bf}q_{bf}\big) - \boldsymbol{N}_{12}\big(\boldsymbol{H}_{ba}\mu\dot{q}_{bf} + \boldsymbol{H}_{bb}\dot{\boldsymbol{q}}_{oj\delta}\big) + \boldsymbol{N}_{12}\begin{bmatrix} \tau_0 \\ \boldsymbol{K}_{mf}\boldsymbol{\sigma}_f \\ -\boldsymbol{K}_\delta\boldsymbol{\delta} \end{bmatrix}, \tag{14}$$

$$\ddot{\boldsymbol{q}}_{oj\delta} = -\boldsymbol{N}_{21}\big(\boldsymbol{H}_{aa}\mu\dot{q}_{bf} + \boldsymbol{H}_{ab}\dot{\boldsymbol{q}}_{oj\delta} + k_{bf}q_{bf}\big) - \boldsymbol{N}_{22}\big(\boldsymbol{H}_{ba}\mu\dot{q}_{bf} + \boldsymbol{H}_{bb}\dot{\boldsymbol{q}}_{oj\delta}\big) + \boldsymbol{N}_{22}\begin{bmatrix} \tau_0 \\ \boldsymbol{K}_{mf}\boldsymbol{\sigma}_f \\ -\boldsymbol{K}_\delta\boldsymbol{\delta} \end{bmatrix}. \tag{15}$$

Consider the case when μ tends to 0, k_b and $\boldsymbol{K}_m$ tend to infinity and q_b tends to 0, we can see that the joint rotation angle $\boldsymbol{q}_j = \begin{bmatrix} \boldsymbol{q}_1 & \boldsymbol{q}_2 \end{bmatrix}^T$ is approximately equal to the motor rotor rotation angle $\boldsymbol{q}_m$. Thus, when $\mu = 0$, the robot can be considered as a rigid system. Let $\Re$ be an arbitrary variable and $\overline{\Re}$ denotes the new expression for $\Re$ as μ tends to 0. To find the dynamics model of the slow subsystem, let $\mu = 0$, from Eqs. (14) and (15) we have

$$0 = -\overline{\boldsymbol{N}}_{11}\overline{\boldsymbol{H}}_{ab}\dot{\boldsymbol{q}}_{oj\delta} - \overline{\boldsymbol{N}}_{11}k_{bf}\overline{q}_{bf} - \overline{\boldsymbol{N}}_{12}\overline{\boldsymbol{H}}_{bb}\dot{\boldsymbol{q}}_{oj\delta} + \overline{\boldsymbol{N}}_{12}\begin{bmatrix} \tau_0 \\ \boldsymbol{K}_{mf}\overline{\boldsymbol{\sigma}}_f \\ -\boldsymbol{K}_\delta\boldsymbol{\delta} \end{bmatrix}, \tag{16}$$

$$\ddot{\boldsymbol{q}}_{oj\delta} = -\overline{\boldsymbol{N}}_{21}\overline{\boldsymbol{H}}_{ab}\dot{\boldsymbol{q}}_{oj\delta} - \overline{\boldsymbol{N}}_{21}k_{bf}\overline{q}_{bf} - \overline{\boldsymbol{N}}_{22}\overline{\boldsymbol{H}}_{bb}\dot{\boldsymbol{q}}_{oj\delta} + \overline{\boldsymbol{N}}_{22}\begin{bmatrix} \tau_0 \\ \boldsymbol{K}_{mf}\overline{\boldsymbol{\sigma}}_f \\ -\boldsymbol{K}_\delta\boldsymbol{\delta} \end{bmatrix}. \tag{17}$$

The total controller of the drive motor with joint flexibility compensation is designed as

$$\boldsymbol{\tau}_m = (\boldsymbol{I} + \boldsymbol{K}_c)\,\boldsymbol{\tau}_n - \boldsymbol{K}_c\boldsymbol{\tau}, \tag{18}$$

where $\boldsymbol{I} \in \mathbf{R}^{2\times 2}$ is the unit matrix, $\boldsymbol{K}_c \in \mathbf{R}^{2\times 2}$ is the symmetric positive definite flexible compensation matrix and $\boldsymbol{\tau}_n = \boldsymbol{\tau}_{ns} + \boldsymbol{\tau}_{nf}$ is the controller to be designed. $\boldsymbol{\tau}_{ns} \in \mathbf{R}^{2\times 1}$ is the slow sub-controller, and $\boldsymbol{\tau}_{nf} \in \mathbf{R}^{2\times 1}$ is the fast sub-controller.

By substituting controller $\boldsymbol{\tau}_m$, $\boldsymbol{\sigma}_f = \boldsymbol{\sigma}/\mu$ and $\mu = 0$ into Eq. (7), we get

$$\boldsymbol{K}_{mf}\overline{\boldsymbol{\sigma}}_f = \boldsymbol{\tau}_{ns} - (\boldsymbol{I} + \boldsymbol{K}_c)^{-1}\boldsymbol{J}_m\ddot{\boldsymbol{q}}_j, \tag{19}$$

By substituting Eqs. (16), (18) and (19) into Eq. (17), we have the dynamics model of the slow subsystem containing $\boldsymbol{q}$ and $\boldsymbol{\delta}$ as

$$\boldsymbol{R}(\boldsymbol{q}_{oj\delta})\,\ddot{\boldsymbol{q}}_{oj\delta} + \boldsymbol{S}(\boldsymbol{q}_{oj\delta}, \dot{\boldsymbol{q}}_{oj\delta})\,\dot{\boldsymbol{q}}_{oj\delta} + \boldsymbol{\xi}_{oj\delta} = \boldsymbol{\tau}_{oj\delta}, \tag{20}$$

where $\boldsymbol{R}(\boldsymbol{q}_{oj\delta}) = \overline{\boldsymbol{D}}_{bb} + \begin{bmatrix} \boldsymbol{0} & \boldsymbol{0} & & \boldsymbol{0} \\ \boldsymbol{0} & (\boldsymbol{I} + \boldsymbol{K}_c)^{-1}\boldsymbol{J}_m & \boldsymbol{0} \\ \boldsymbol{0} & \boldsymbol{0} & & \boldsymbol{0} \end{bmatrix}$, $\boldsymbol{S}(\boldsymbol{q}_{oj\delta}, \dot{\boldsymbol{q}}_{oj\delta}) = \overline{\boldsymbol{H}}_{bb}$, $\boldsymbol{\xi}_{oj\delta} = \begin{bmatrix} \boldsymbol{0}^T & (\boldsymbol{K}_\delta\boldsymbol{\delta})^T \end{bmatrix}^T$,

$\boldsymbol{\tau}_{oj\delta} = \begin{bmatrix} (\boldsymbol{\tau}_{oj})^T & \boldsymbol{0}^T \end{bmatrix}^T$, and $\boldsymbol{\tau}_{oj} = \begin{bmatrix} \tau_0 & \boldsymbol{\tau}_{ns}^T \end{bmatrix}^T$.

Denote the fast subsystem state variable as $\boldsymbol{q}_f = \begin{bmatrix} q_{f1} & q_{f2} & \boldsymbol{q}_{f3}^T & \boldsymbol{q}_{f4}^T \end{bmatrix}^T$, and we have $q_{f1} = q_{bf} - \overline{q}_{bf}$, $q_{f2} = \sqrt{\mu}\dot{q}_{bf}$, $\boldsymbol{q}_{f3} = \boldsymbol{\sigma} - \overline{\boldsymbol{\sigma}}_f$ and $\boldsymbol{q}_{f4} = \sqrt{\mu}\dot{\boldsymbol{\sigma}}_f$. $\boldsymbol{q}_f$ is derived with respect to t_f, and the dynamics model of the fast subsystem containing q_b and $\boldsymbol{\sigma}$ is obtained by combining Eq. (14), controllers $\boldsymbol{\tau}_m$, $\boldsymbol{\sigma}_f = \boldsymbol{\sigma}/\mu$ and Eq. (7), as

$$\mathrm{d}\boldsymbol{q}_f/\mathrm{d}t_f = \boldsymbol{A}_f\boldsymbol{q}_f + \boldsymbol{B}_f\boldsymbol{\tau}_{nf}, \tag{21}$$

where $\boldsymbol{A}_f = \begin{bmatrix} 0 & 1 & \boldsymbol{0} & \boldsymbol{0} \\ -\overline{\boldsymbol{N}}_{11}k_{bf} & 0 & \boldsymbol{N}_{12}^*\boldsymbol{K}_{mf} & \boldsymbol{0} \\ \boldsymbol{0} & \boldsymbol{0} & \boldsymbol{0} & \boldsymbol{I} \\ \boldsymbol{0} & \boldsymbol{0} & -\boldsymbol{J}_m^{-1}(\boldsymbol{I} + \boldsymbol{K}_c)\,\boldsymbol{K}_{mf} & \boldsymbol{0} \end{bmatrix}$, $\boldsymbol{B}_f = \begin{bmatrix} \boldsymbol{0} \\ \boldsymbol{0} \\ \boldsymbol{0} \\ \boldsymbol{J}_m^{-1}(\boldsymbol{I} + \boldsymbol{K}_c) \end{bmatrix}$, $\boldsymbol{N}_{12}^*$ is the row vector con-

sisting of the elements of the second and third terms of $\overline{\boldsymbol{N}}_{12}$.

3.2. Dynamical model properties

From Eq. (20), it can be seen that the motion of the base and joints of the slow subsystem and the links vibration are coupled with each other. In order to control the base attitude and the joints, this

section decouples the slow subsystem into a fully driven rigid subsystem and designs the control algorithm. Among them, $\boldsymbol{R}(\boldsymbol{q}_{oj\delta})$ and $\boldsymbol{S}(\boldsymbol{q}_{oj\delta}, \dot{\boldsymbol{q}}_{oj\delta})$ are written as $\begin{bmatrix} \boldsymbol{R}_{11} & \boldsymbol{R}_{12} \\ \boldsymbol{R}_{21} & \boldsymbol{R}_{22} \end{bmatrix}$ and $\begin{bmatrix} \boldsymbol{S}_{11} & \boldsymbol{S}_{12} \\ \boldsymbol{S}_{21} & \boldsymbol{S}_{22} \end{bmatrix}$, respectively. $\boldsymbol{R}_{11}, \boldsymbol{S}_{11} \in \mathbb{R}^{3\times3}, \boldsymbol{R}_{12}, \boldsymbol{S}_{12} \in \mathbb{R}^{3\times4}, \boldsymbol{R}_{21}, \boldsymbol{S}_{21} \in \mathbb{R}^{4\times3}$, and $\boldsymbol{R}_{22}, \boldsymbol{S}_{22} \in \mathbb{R}^{4\times4}$. The fully driven rigid subsystem dynamic model is obtained from Eq. (20), as

$$\boldsymbol{M}(\delta, \boldsymbol{q})\,\ddot{\boldsymbol{q}} + \boldsymbol{C}\big(\delta, \dot{\delta}, \boldsymbol{q}, \dot{\boldsymbol{q}}\big)\,\dot{\boldsymbol{q}} + \boldsymbol{\kappa}\big(\delta, \dot{\delta}, \boldsymbol{q}, \dot{\boldsymbol{q}}\big) = \boldsymbol{\tau}_{oj}, \tag{22}$$

where $\boldsymbol{M} = \boldsymbol{R}_{11} - \boldsymbol{R}_{12}\boldsymbol{R}_{22}^{-1}\boldsymbol{R}_{21}, \boldsymbol{C} = \boldsymbol{S}_{11} - \boldsymbol{R}_{12}\boldsymbol{R}_{22}^{-1}\boldsymbol{S}_{21}$, and $\boldsymbol{\kappa} = \big(\boldsymbol{S}_{12} - \boldsymbol{R}_{12}\boldsymbol{R}_{22}^{-1}\boldsymbol{S}_{22}\big)\dot{\delta} - \boldsymbol{R}_{12}\boldsymbol{R}_{22}^{-1}\boldsymbol{K}_8\delta$ is the system dynamics nonlinear term.

According to Kelly *et al.* [30], Eq. (22) has several fundamental properties as follows:

Property 1. The inertia matrix $\boldsymbol{M}(\boldsymbol{x})$ is symmetric positive definite and satisfies the following inequalities:

$$\lambda_m(\boldsymbol{M})\,\|\boldsymbol{y}\|^2 \leq \boldsymbol{y}^T\boldsymbol{M}(\boldsymbol{x})\,\boldsymbol{y} \leq \lambda_M(\boldsymbol{M})\,\|\boldsymbol{y}\|^2 \;\forall \boldsymbol{y} \in \mathbb{R}^{3\times1}, \tag{23}$$

where $\lambda_m(\cdot)$ and $\lambda_M(\cdot)$ represent the minimum and maximum eigenvalues of the matrix, respectively, and $\|\cdot\|$ represents the 2-norm.

Property 2. The centrifugal-Coriolis matrix $\boldsymbol{C} \in \mathbb{R}^{3\times3}$ satisfies the following relationship:

$$\boldsymbol{C}(\boldsymbol{x}, \boldsymbol{y})\,\boldsymbol{z} = \boldsymbol{C}(\boldsymbol{x}, \boldsymbol{z})\,\boldsymbol{y}\,\forall \boldsymbol{y}, \boldsymbol{z} \in \mathbb{R}^{3\times1}, \tag{24}$$

$$C_m\,\|\boldsymbol{y}\| \leq \|\boldsymbol{C}(\boldsymbol{x}, \boldsymbol{y})\| \leq C_M\,\|\boldsymbol{y}\| \;\forall \boldsymbol{y} \in \mathbb{R}^{3\times1}, \tag{25}$$

where C_m and C_M are known positive constants.

Property 3. The matrix $\dot{\boldsymbol{M}}(\boldsymbol{x}) - 2\boldsymbol{C}(\boldsymbol{x}, \dot{\boldsymbol{x}})$ is skew-symmetric, which implies that

$$\boldsymbol{y}^T\big[\dot{\boldsymbol{M}}(\boldsymbol{x}) - 2\boldsymbol{C}(\boldsymbol{x}, \dot{\boldsymbol{x}})\big]\boldsymbol{y} = \boldsymbol{0}\,\forall \boldsymbol{y} \in \mathbb{R}^{3\times1}. \tag{26}$$

Property 4. There must exist known positive constants $k_M, k_{C1}, k_{C2}, k_{C3}$ and k_{C4} for all $\boldsymbol{x}, \boldsymbol{y}, \boldsymbol{z}, \boldsymbol{x}_1, \boldsymbol{y}_1, \boldsymbol{x}_2, \boldsymbol{y}_2 \in \mathbb{R}^{3\times1}$ fulfilling

$$\|\boldsymbol{M}(\boldsymbol{x})\,\boldsymbol{z} - \boldsymbol{M}(\boldsymbol{y})\,\boldsymbol{z}\| \leq k_M\,\|\mathbf{Tanh}(\boldsymbol{x} - \boldsymbol{y})\|\,\|\boldsymbol{z}\|, \tag{27}$$

$$\|\boldsymbol{C}(\boldsymbol{x}_1, \boldsymbol{y}_1)\,\boldsymbol{z} - \boldsymbol{C}(\boldsymbol{x}_2, \boldsymbol{y}_2)\,\boldsymbol{z}\| \leq k_{C1}\,\|\mathbf{Tanh}(\boldsymbol{y}_1 - \boldsymbol{y}_2)\|\,\|\boldsymbol{z}\| + k_{C2}\,\|\boldsymbol{y}_1\|\,\|\mathbf{Tanh}(\boldsymbol{x}_1 - \boldsymbol{x}_2)\|\,\|\boldsymbol{z}\|, \tag{28}$$

$$\|\boldsymbol{\kappa}(\boldsymbol{x}_1, \boldsymbol{y}_1) - \boldsymbol{\kappa}(\boldsymbol{x}_2, \boldsymbol{y}_2)\| \leq k_{C3}\,\|\boldsymbol{y}_1 - \boldsymbol{y}_2\| + k_{C4}\,\|\boldsymbol{y}_1\|\,\|\mathbf{Tanh}(\boldsymbol{x}_1 - \boldsymbol{x}_2)\|, \tag{29}$$

where $k_M, k_{C1}, k_{C2}, k_{C3}$ and k_{C4} are obtained according to Kelly. $\boldsymbol{\xi} = \begin{bmatrix} \xi_1 & \xi_2 & \xi_3 \end{bmatrix}^T \in \mathbb{R}^{3\times1}$, and $\mathbf{Tanh}(\boldsymbol{\xi}) = \begin{bmatrix} \tanh(\xi_1) & \tanh(\xi_2) & \tanh(\xi_3) \end{bmatrix}^T$, where $\boldsymbol{\xi}$ is an arbitrary vector.

4. ISMC-IOR

4.1. SMC-IOR base on desired trajectory

The continuous differentiable periodic expectation trajectory satisfies the bounded condition

$$\|\dot{\boldsymbol{q}}_d\| \leq V_M, \quad \text{and} \quad \|\ddot{\boldsymbol{q}}_d\| \leq A_M, \tag{30}$$

where V_M and A_M are, respectively, the upper bound of the expected velocity and the acceleration norm.

For the convenience of analysis, define $N \in \mathbf{R}^{3 \times 1}$ as

$$N(q, \dot{q}) = M(\delta, q)\ddot{q}_d + C(\delta, \dot{\delta}, q, \dot{q})\dot{q} + \kappa(\delta, \dot{\delta}, q, \dot{q}). \tag{31}$$

Let $N_d = N(q_d, \dot{q}_d)$, where N_d is a periodic function with period T. Expanded N_d in Fourier series as

$$N_d = \bar{a}_0 + \sum_{k=1}^{\infty}\left[\bar{a}_k \cos(k\omega t) + \bar{b}_k \sin(k\omega t)\right], \tag{32}$$

where $\omega = 2\pi/T$ is the angular frequency. $\bar{a}_0, \bar{a}_k$ and $\bar{b}_k$ are the unknown constant vectors.

Define the filtered tracking error $\eta = \dot{e} + \mathbf{Tanh}(e) + \mathbf{Tanh}(v)$, where $e = q_d - q$ is the trajectory tracking error and $v \in \mathbf{R}^{3 \times 1}$ is the filter vector. For the rigid subsystem Eq. (22), design the algorithm of sliding mode control with input restriction, output feedback and repetitive learning based on the desired trajectory (SMC-IOR-D) as

$$\tau_{oj} = K_0 \mathbf{Sgn}\left(\mathbf{Tanh}(e) + \alpha e_f\right) - (k'+1)\,\mathbf{Tanh}(v) + \mathbf{Tanh}(e) + \mathbf{Sat}\left(Q_0 z_0 + \sum_{k=1}^{N} Q_k \dot{z}_k\right), \tag{33}$$

$$\begin{cases} \mathbf{Tanh}(v) = p_1 - (k'+1)\,e \\ \dot{p}_1 = -k'\mathbf{Tanh}(e) - (k'+2)\,\mathbf{Tanh}(v) - \alpha^{-1}e_f \\ p_1(0) = (k'+1)\,e(0) \end{cases}, \tag{34}$$

$$\begin{cases} e_f = p_2 + \alpha^{-1}(e - \mathbf{Tanh}(e)) \\ \dot{p}_2 = \alpha^{-1}\mathbf{Tanh}(v) - e_f \\ p_2(0) = \alpha^{-1}(\mathbf{Tanh}(e(0)) - e(0)) \end{cases}, \tag{35}$$

$$\begin{cases} z_0 = p_0 + Q_0 e \\ \dot{p}_0 = Q_0(\mathbf{Tanh}(e) + \mathbf{Tanh}(v)) \end{cases}, \tag{36}$$

$$\begin{cases} \dot{z}_k = p_k + Q_k e \\ \dot{p}_k = Q_k(\mathbf{Tanh}(e) + \mathbf{Tanh}(v)) - k^2\omega^2 z_k \end{cases} \quad k = 1, \cdots N, \tag{37}$$

where $K_0 \in \mathbb{R}^{3 \times 3}$ is a constant diagonal matrix, $e_f \in \mathbb{R}^{3 \times 1}$ is a filter vector and α and k' are positive constants. $Q_0, Q_k \in \mathbb{R}^{3 \times 3}$ are constant positive definite diagonal matrices, $Q_0 z_0 + \sum_{k=1}^{N} Q_k \dot{z}_k$ is the repetitive learning controller (RC), and N is the number of harmonic oscillator terms. $\mathbf{Sgn}(\boldsymbol{\xi}) = \begin{bmatrix} \mathrm{sgn}(\xi_1) & \mathrm{sgn}(\xi_2) & \mathrm{sgn}(\xi_3) \end{bmatrix}^T$, $\mathbf{Sat}(\boldsymbol{\xi}) = \begin{bmatrix} \mathrm{sat}(\xi_1) & \mathrm{sat}(\xi_2) & \mathrm{sat}(\xi_3) \end{bmatrix}^T$, $\boldsymbol{\xi} \in \mathbb{R}^{3 \times 1}$ is an arbitrary vector. $\mathbf{Sat}(\cdot)$ is a saturation function whose elements are as follows:

$$\mathrm{sat}(\xi_{i'}) = \begin{cases} \xi_{i'}, & |\xi_{i'}| \le \beta_{i'} \\ \beta_{i'}\mathrm{sgn}(\xi_{i'}), & |\xi_{i'}| > \beta_{i'} \end{cases} \quad \forall \xi_{i'} \in \mathbb{R}, i' = 1, 2, 3, \tag{38}$$

where $\beta_{i'}$ is the maximum threshold value of the saturation function.

Take the derivative of η, left multiply both sides of the resultant equation by $M(\delta, q)$ and substituting $e = q_d - q$, Eqs. (22), (31) and (34) into the right side of the equation, then we have

$$M(\delta, q)\dot{\eta} = -k'M(\delta, q)\eta - M(\delta, q)\left(I_3 - \mathbf{Sech}^2(e)\right)\eta + \tilde{N} + N_d - \tau_{oj} - \frac{1}{2}\dot{M}(\delta, q)\eta, \tag{39}$$

$$\tilde{N} = N - N_d - M(\delta, q)\left[\mathbf{Sech}^2(e)\left(\mathbf{Tanh}(e) + \mathbf{Tanh}(v)\right) + \mathbf{Tanh}(v) - \mathbf{Tanh}(e) + \alpha^{-1}e_f\right] + \frac{1}{2}\dot{M}(\delta, q)\eta. \tag{40}$$

Convert Eq. (40) into the normal form, and according to $e = q_d - q$, Properties 1−4 and Eq. (30), it is obtained from the expression of η that

$$\left\| \tilde{N} \right\| \leq 4\lambda_{M1} \left\| z \right\| + \lambda_{M2} \left\| z \right\|^2 = (4\lambda_{M1} + \lambda_{M2} \left\| z \right\|) \left\| z \right\| = \rho(\left\| z \right\|) \left\| z \right\|, \tag{41}$$

where $\lambda_{M1} = \max\{\wp_1, \wp_2, \wp_3, \wp_4\}$, $\lambda_{M2} = 8C_M$, $z = \begin{bmatrix} \mathbf{Tanh}^T(e) & e_f^T & \mathbf{Tanh}^T(v) & \eta^T \end{bmatrix}^T$. $\wp_1 = k_M A_M + k_{C2} V_M^2 + 2C_M V_M + k_{C4} V_M + \lambda_M(M) + k_{C3}$, $\wp_2 = 2C_M V_M + \frac{1}{2}\lambda_M(\dot{M}) + k_{C3}$, $\wp_3 = \frac{\lambda_M(M)}{\alpha}$, $\wp_4 = 2C_M V_M + \lambda_M(M) + k_{C3}$. $\rho(\left\| z \right\|) \in \mathbb{R}$ is the positive definite invertible non-decreasing function.

Lemma 1. *Define the auxiliary intermediate variable $L_n(t) \in \mathbb{R}$ as shown below*

$$L_n(t) = \eta^T \left[f_n(t) - K_0 \mathbf{sgn}(\mathbf{Tanh}(e) + \alpha e_f) \right], \tag{42}$$

If K_{0ii} satisfies sufficient $K_{0ii} > \left\| f_n(t) \right\|_\infty + \left\| \dot{f}_n(t) \right\|_\infty$, then

$$\int_0^t L_n(\tau)\,\mathrm{d}\tau \leq \xi_n, \tag{43}$$

where K_{0ii} denotes the i-th element on the diagonal of the diagonal matrix K_0. $K_{0ii} = \begin{bmatrix} K_{011} & K_{022} & K_{033} \end{bmatrix}^T$, $f_n(t), \dot{f}_n(t) \in l_\infty$, and $\xi_n = \sum_{i=1}^n K_{0ii}|\tanh(e_i(0))| - \mathbf{Tanh}^T(e(0)) f_n(0)$, $n = 1, 2$.

Proof. See Appendix A. □

Thus, the stability theorem for SMC-IOR-D is formulated as follows:

Theorem 1. *When Eqs. (33)−(37) of SMC-IOR-D are under the input constraints from Eq. (44), if the controller parameters meet the sufficient conditions shown in Eqs. (45)−(48), the asymptotic stable trajectory tracking control of the FBFLFJ space robot can be realized*

$$K_{0ii} + k' + 2 + \beta_i \leq \tau_{oj,i,\max}, \tag{44}$$

$$K_{0ii} > \max\left\{ \left\| f_1(t) \right\|_\infty + \left\| \dot{f}_1(t) \right\|_\infty, \left\| f_2(t) \right\|_\infty + \left\| \dot{f}_2(t) \right\|_\infty \right\}, \tag{45}$$

$$\alpha > 1.5, \tag{46}$$

$$k' = (k_n + 1) / \lambda_m(M), \tag{47}$$

$$k_n > \frac{1}{4\lambda_3} \max\left\{ \rho^2\left(\sqrt{\lambda_{12}/\lambda_{11}} \left\| y_1(0) \right\|\right), \rho^2\left(\sqrt{\lambda_{22}/\lambda_{21}} \left\| y_2(0) \right\|\right), \rho^2(\left\| z(0) \right\|) \right\}, \tag{48}$$

where $\lambda_{11} = 0.5 \min\{1, \lambda_m(M)\}$, $\lambda_{12} = \max\{1, \frac{1}{2}\lambda_M(M)\}$, $\lambda_{21} = \frac{1}{2} \min\{1, \lambda_m(Q_0), \omega^2, \lambda_m(M)\}$, $\lambda_{22} = \frac{1}{2} \max\{2, \lambda_M(Q_0), N^2\omega^2, \lambda_M(M)\}$, $\lambda_3 = 1 - \frac{3}{2\alpha}$, $f_1(t) = N_d - B \cdot \mathbf{sgn}(Q_0 z_0 + \sum_{k=1}^N Q_k \dot{z}_k)$, and $f_2(t) = \sum_{k=N+1}^\infty \left[\overline{a}_k \cos(k\omega t) + \overline{b}_k \sin(k\omega t) \right]$.

Proof. See Appendix B. □

4.2. SMC-IOR based on hybrid trajectory

The SMC-IOR-D in the previous section achieves asymptotic stable tracking of the base attitude and joint angle, but the vibration of the flexible link is not suppressed. In this section, we use the concept of virtual control force to modify the original desired trajectory and generate a hybrid trajectory q_h that reflects both the flexible vibration of the link and the rigid motion of the system. Based on this, the sliding mode control with input restriction, output feedback and repetitive learning based on the hybrid trajectory (SMC-IOR-H) is designed to achieve the dual functions of motion tracking and simultaneous suppression of the links vibration. The virtual force $F \in \mathbb{R}^{3\times1}$ is introduced, and the error between the desired trajectory and the hybrid trajectory is $e_h = q_d - q_h$, which is generated by the second-order

command generator $\ddot{e}_h + a\dot{e}_h + be_h = F$, where $a, b \in \mathbb{R}^{3\times3}$ are the constant positive definite diagonal matrix.

The hybrid error is defined as $e_r = q_h - q$, and the hybrid filter tracking error is defined as $\eta_r = \dot{e}_r + \text{Tanh}(e_r) + \text{Tanh}(v_r)$. v_r and e_{fr} are the hybrid filter vectors. Then, the SMC-IOR-H is obtained as follows:

$$(\boldsymbol{\tau}_{oj})_r = K_0 \text{Sgn}(\text{Tanh}(e_r) + \alpha e_{fr}) - (k'+1)\,\text{Tanh}(v_r) + \text{Tanh}(e_r) + \text{Sat}\left(Q_0 z_{0r} + \sum_{k=1}^{N} Q_k \dot{z}_{kr}\right), \quad (49)$$

$$\begin{cases} \text{Tanh}(v_r) = p_{1r} - (k'+1)\,e_r \\ \dot{p}_{1r} = -k'\text{Tanh}(e_r) - (k'+2)\,\text{Tanh}(v_r) - \alpha^{-1}e_{fr} \\ p_{1r}(0) = (k'+1)\,e_r(0) \end{cases} \quad (50)$$

$$\begin{cases} e_{fr} = p_{2r} + \alpha^{-1}(e_r - \text{Tanh}(e_r)) \\ \dot{p}_{2r} = \alpha^{-1}\text{Tanh}(v_r) - e_{fr} \\ p_{2r}(0) = \alpha^{-1}(\text{Tanh}(e_r(0)) - e_r(0)) \end{cases} \quad (51)$$

$$\begin{cases} z_{0r} = p_{0r} + Q_0 e_r \\ \dot{p}_{0r} = Q_0(\text{Tanh}(e_r) + \text{Tanh}(v_r)) \end{cases}, \quad (52)$$

$$\begin{cases} \dot{z}_{kr} = p_{kr} + Q_k e_r \\ \dot{p}_{kr} = Q_k(\text{Tanh}(e_r) + \text{Tanh}(v_r)) - k^2\omega^2 z_{kr} \end{cases} \quad k = 1, \cdots N. \quad (53)$$

Defining the state variable as $q_s = \begin{bmatrix} \delta^T & e^T & \dot{\delta}^T & \dot{e}^T \end{bmatrix}^T$, the equation of state is obtained from Eqs. (49)–(53) and Eq. (22) as follows:

$$\dot{q}_s = A_s q_s + B_s F + L_s, \quad (54)$$

where $A_s = \begin{bmatrix} \mathbf{0} & \mathbf{0} & I & \mathbf{0} \\ \mathbf{0} & \mathbf{0} & \mathbf{0} & I \\ -R_{22}^{-1}K_\delta & -R_{22}^{-1}R_{21}b & -R_{22}^{-1}S_{22} & -R_{22}^{-1}R_{21}a \\ \mathbf{0} & -b & \mathbf{0} & -a \end{bmatrix}$, $B_s = \begin{bmatrix} \mathbf{0} \\ \mathbf{0} \\ R_{22}R_{21} \\ I \end{bmatrix}$, and $L_s = \begin{bmatrix} \mathbf{0} \\ \mathbf{0} \\ R_{22}^{-1}R_{21}(G - \ddot{q}_d) - R_{22}^{-1}S_{21}\dot{q} \\ G \end{bmatrix}$.

If L_s satisfies the following conditions:

$$\frac{\|L_s(t)\|_E}{\|q_s\|_E} \le \frac{1}{2\,\|N_s^{-1}\|_s\,\|P_s\|_s} = \frac{\lambda_{\min}(N_s)}{2\lambda_{\max}(P_s)}, \forall q_s \in \mathbf{R}^{3\times1}, \quad (55)$$

then the virtual force F is

$$F = -R_s^{-1}B_s^T P_s q_s. \quad (56)$$

In Eq. (56), $R_s > 0$, and P_s is the solution of Riccati equation $P_s A_s + A_s^T P_s - P_s B_s R_s^{-1} B_s^T P_s + Q_s = \mathbf{0}$. Constructing the Lyapunov function $V(q_s) = q_s^T P_s q_s$, $V(q_s)$ is derived and combining with Eqs. (55) and (56) yields $\dot{V}(q_s) \le -\left(q_s^T N_s q_s - \lambda_{\min}(N_s)\,\|q_s\|^2\right) \le 0$, so the system is stable.
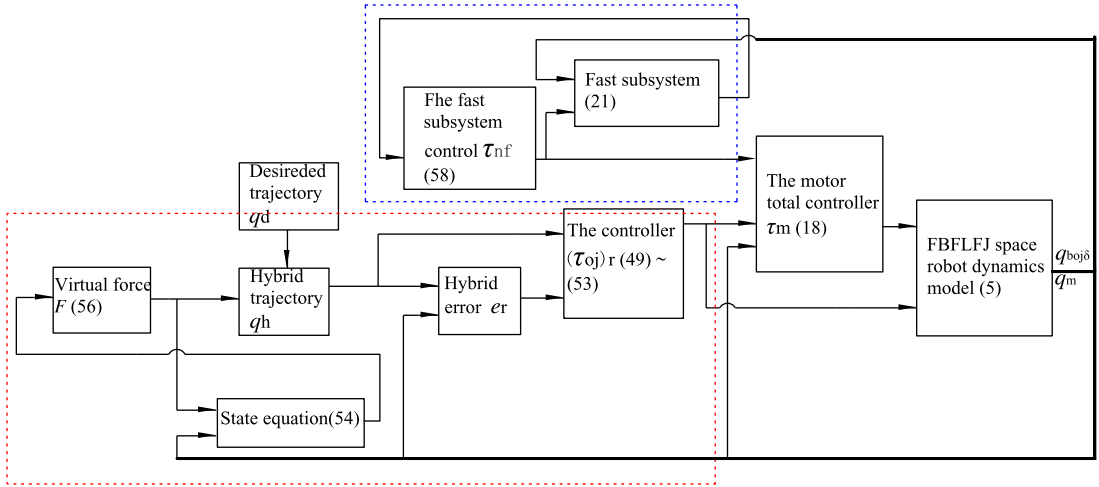
Figure 4. *Integrated sliding mode control with input restriction, output feedback and repetitive learning.*

4.3. Multiple flexible suppression control based on linear quadratic optimal method

As analyzed above, the state equation q_f at the fast time scale t_f is shown in Eq. (21). The performance index function is constructed as

$$J_{qf} = 0.5 \int_0^\infty \left(q_f^T Q_f q_f + \tau_{nf}^T R_f \tau_{nf} \right) \mathrm{d}t_f. \tag{57}$$

In Eq. (57), symmetric matrix $Q_f \geq 0, R_f > 0$. The optimal control of the fast subsystem is designed as

$$\tau_{nf} = -R_f^{-1} B_f^T P_f q_f, \tag{58}$$

where P_f is the solution of the Riccati equation $P_f A_f + A_f^T P_f - P_f B_f R_f^{-1} B_f^T P_f + Q_f = 0$.

Then, ISMC-IOR is composed of SMC-IOR-H, virtual force Eq. (56), fast sub-controller Eq. (58) and motor general controller Eq. (18). The overall scheme of this controller is shown in flowchart Fig. 4, where the blue dashed area is the fast subsystem controller and the red dashed area is the slow subsystem controller. According to the above analysis, the implementation of the ISMC-IOR does not need the dynamic model information of space robot and the motion speed information of base and joint, and can meet the requirements of limited driving torque of FBFLFJ space robot.

5. Simulation

Taking the FBFLFJ space robot shown in Fig. 1 as an example, the simulation is carried out. The size of the base is $l_0 = 1.5$ m, the mass of the base is $m_0 = 40$ kg, the inertia moment of the base is $J_0 = 30$ kg $\cdot$ m^2 and the elastic coefficient of the base is $k_b = 500$ N/m. The density of link B_1 is $\rho_1 = 3.5$ kg/m, the density of link B_2 is $\rho_2 = 1.1$ kg/m, the length of the link is $l_i = 1.5$ m and the bending stiffness of the link is EI$_i = 100$ N/m^2. At joint i, the motor rotor rotational inertia is $J_{mi} = 0.1$ kg $\cdot$ m^2 and the joint elasticity coefficient is $k_{mi} = 50$ Nm/rad, $i = 1, 2$. Before the controller is turned on, the FBFLFJ space robot base and joints do not move, and the base, links and joints do not vibrate. Its initial configuration is $q_b(0) = 0$ m, $q(0) = \begin{bmatrix} 1.1 & 0.7 & 1.4 \end{bmatrix}^T$ rad, $\delta(0) = \begin{bmatrix} 0 & 0 & 0 & 0 \end{bmatrix}$ m, $q_m(0) = \begin{bmatrix} 0.7 & 1.4 \end{bmatrix}^T$ rad, $\dot{q}_b(0) = 0$ m, $\dot{q}(0) = \begin{bmatrix} 0 & 0 & 0 \end{bmatrix}^T$ rad, $\dot{\delta}(0) = \begin{bmatrix} 0 & 0 & 0 & 0 \end{bmatrix}$ m, $\dot{q}_m(0) = \begin{bmatrix} 0 & 0 \end{bmatrix}^T$ rad. Let 0 s be the simulation initial moment. At this time, turn on the controller so that the FBFLFJ robot base and joints track the following desired trajectory:

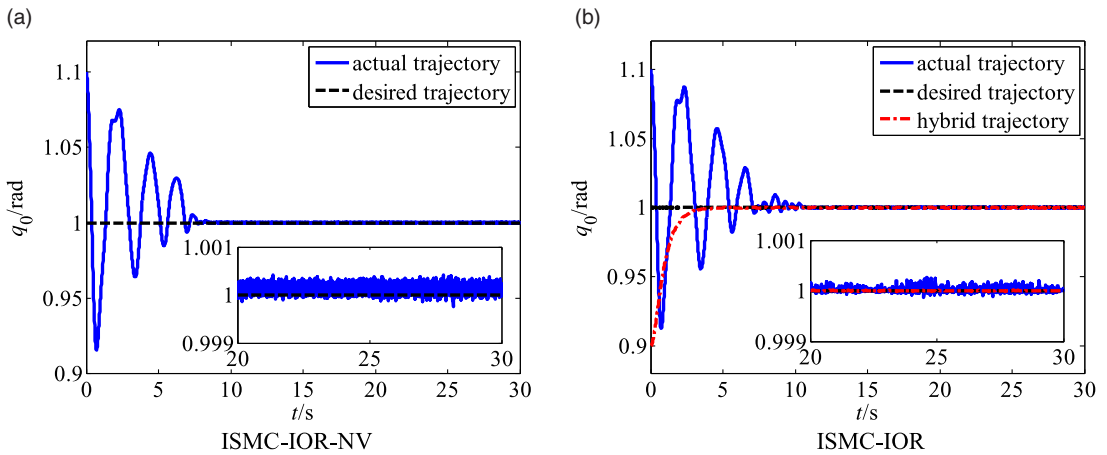$$q_d = \begin{bmatrix} 1 & 0.8 & 1.2 \end{bmatrix}^T \text{ rad.}$$

Figure 5. *Trajectory tracking curve of the FBFLFJ space robot base attitude under two control conditions. (a) ISMC-IOR-NV. (b) ISMC-IOR.*

In order to illustrate the vibration suppression effect on the flexible vibration of the base, links and joints and motion control effect of the base and joints of the FBFLFJ space robot, ISMC-IOR is used to conduct a simulation study, where the controller parameters are $K_0 = \text{diag}(20, 0.5, 0.9)$, $k' = 20$, $\alpha = 5$, $Q_0 = \text{diag}(10, 90, 30)$, $Q_k = \text{diag}(2, 2, 2)$, $N = 3$, $a = b = \text{diag}(5, 5, 5)$. The saturation function thresholds are $\beta_1 = 20$, $\beta_2 = \beta_3 = 40$. The flexible vibration of the FBFLFJ space robot base, links and joints affects the system control accuracy. In order to verify the effect of flexible vibration on the system control accuracy, the flexible suppressors in ISMC-IOR, i.e., the fast sub-controller τ_{nf} and the SMC-IOR-H are turned off, and the ISMC-IOR without vibration suppression (ISMC-IOR-NV) consisting of the SMC-IOR-D and $\tau_m = (I + K_c)\,\tau_{ns} - K_c\tau$ is used for simulation studies. For fairness, all control parameters remained unchanged. The control conditions are divided into ISMC-IOR-NV and ISMC-IOR.

Figure 5 shows the FBFLFJ space robot base attitude trajectory tracking under two control conditions, and Fig. 6 shows the FBFLFJ space robot joints trajectory tracking under two control conditions.

As can be seen from Figs. 5(a) and 6(a), without the flexible vibration suppressor, although the base and joints can track the desired trajectory, they have an obvious vibration trend after stabilization. Among them, joint 1 showed vibration in 0.5–1.5 s, and after 20 s, both the base and the joints have different amplitudes of vibration. From Figs. 5(b) and 6(b), it can be seen that by turning on the flexible vibration suppressor and using ISMC-IOR for controlling, not only the base and joints can accurately track the desired trajectory, but also the vibration of the base and joints has been significantly suppressed.

Figure 7(a) and (b) shows the error convergence rate under ISMC-IOR-NV and ISMC-IOR control conditions, which are calculated by the formula $\log \|q - q_d\|$, and the unit is log(rad). Therefore, the smaller the error convergence rate, the higher the control accuracy of the controller. Furthermore, to verify the high-precision characteristics of the repetitive learning controller in ISMC-IOR, the integrated sliding mode control for motion and vibration (ISMC) algorithm without repetitive learning controller is used to control the FBFLFJ space robot to track the desired trajectory q_d. The slow sub-controller in ISMC is $(\tau_{oj})_r = M(\ddot{q}_h + \lambda_1\dot{e}_r + \lambda_2 s_r) + C\dot{q} + \kappa$, where, $s_r = \dot{e}_r + \lambda_1 e_r$. The control parameters are $\lambda_1 = \lambda_1 = 1$. The rest of the parameters are identical to those of ISMC-IOR. Figure 7(c) shows the error convergence rate under ISMC.

As can be seen from Fig. 7(a) and (b), the minimum error convergence rate is about -3.2 when the flexible vibration suppressor is turned off, while the minimum error convergence rate is about -4.7 when the flexible vibration suppressor is turned on, and the accuracy of ISMC-IOR control is significantly higher than that of ISMC-IOR-NV. It shows that the flexible vibration seriously affects the control accuracy of the system, and the ISMC-IOR proposed in this paper can improve the control quality of the system. In addition, it can be seen from Fig. 7(c) that the system error convergence rate mean value
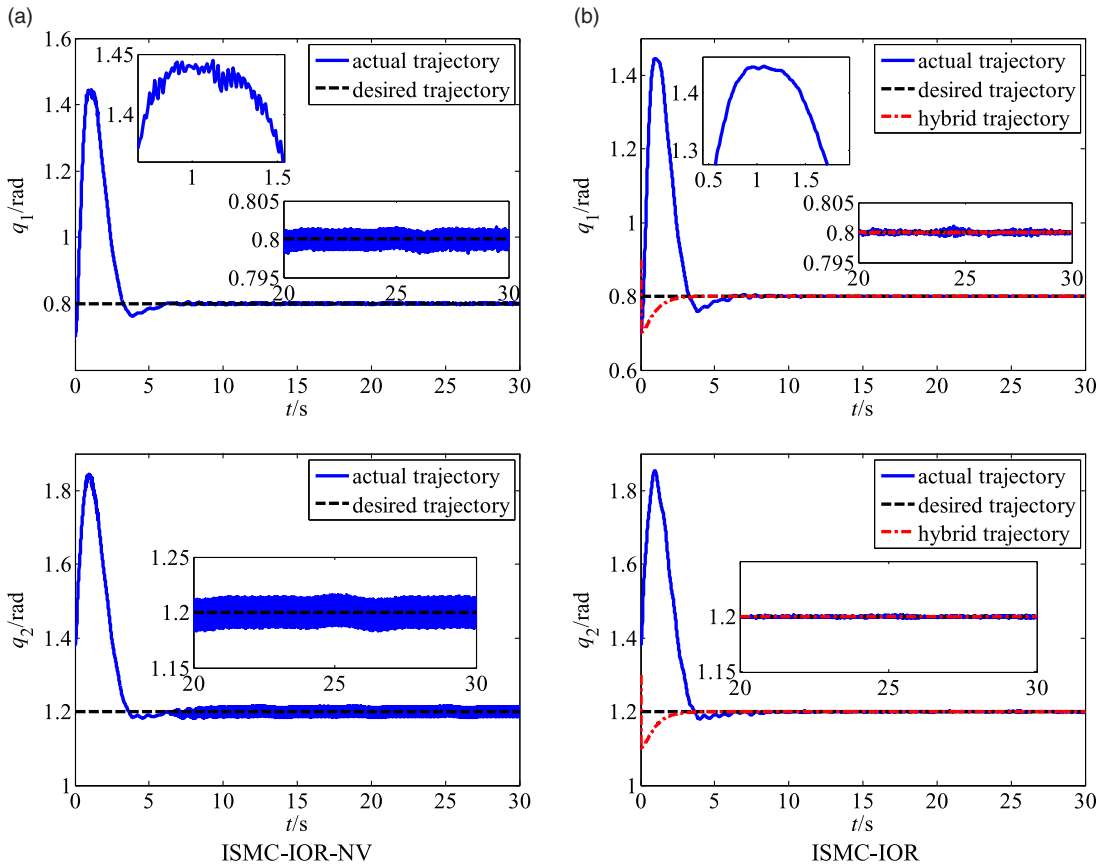
Figure 6. *Trajectory tracking curve of the FBFLFJ space robot joints under two control conditions.*
(a) ISMC-IOR-NV. (b) ISMC-IOR.

under ISMC is about -2.8, which is significantly lower than the error convergence rate mean value of -3.8 under ISMC-IOR, see Fig. 7(b); therefore, ISMC-IOR has higher control accuracy than ISMC in tracking repetitive signals, calibrating the effectiveness of the repetitive controller. In order to clarify the error convergence under the three control conditions, the error convergence values for the three control cases at any moment are analyzed according to Fig. 7, as shown in Table I.

As can be seen from Table I, the error convergence value of the system under ISMC-IOR control is the smallest, which proves the effectiveness of the controller proposed in this paper in high-precision tracking control.

In order to verify the effect of the control algorithm proposed in this paper on the flexible vibration suppression of the base and joints of the system, the following simulation analysis is conducted. Figure 8 shows the flexible vibration curves of the base under the two control conditions, and Figs. 9 and 10 show the flexible vibration curves of joint 1 and joint 2 under the two control conditions.

As can be seen from Fig. 8, the amplitude of the base reached 0.1 m when turning on the controller. With ISMC-IOR-NV control, the amplitude of the base was maintained at 0.0014 m after 20–30 s, while with ISMC-IOR control, the amplitude of the base gradually decreased and was suppressed to within 0.0005 m at 30 s. The vibration frequency was also decreased. From Fig. 9(a), it can be seen that under the ISMC-IOR-NV control, the amplitude of joint 1 reached 3 rad at 2 s and maintained at 1 rad after 10 s. The amplitude of joint 2 reached 1.2 rad at 2 s and maintained at 1.8 rad after 10 s. From Fig. 9(b), it can be seen that under the ISMC-IOR control, the initial amplitude of the joint 1 is 1.2 rad, which is maintained within 0.17 rad after stabilization; the initial amplitude of the joint 2 is 0.6 rad,

Table I. *Tracking error convergence value under three control conditions.*

No.	Control conditions	15s	20s	25s	30s	Average
1	ISMC-IOR-NV	−2.10	−1.95	−1.90	−2.00	−1.99
2	ISMC-IOR	−3.10	−3.20	−2.90	−3.00	−3.05
3	ISMC	−2.20	−2.25	−2.35	−2.25	−2.26
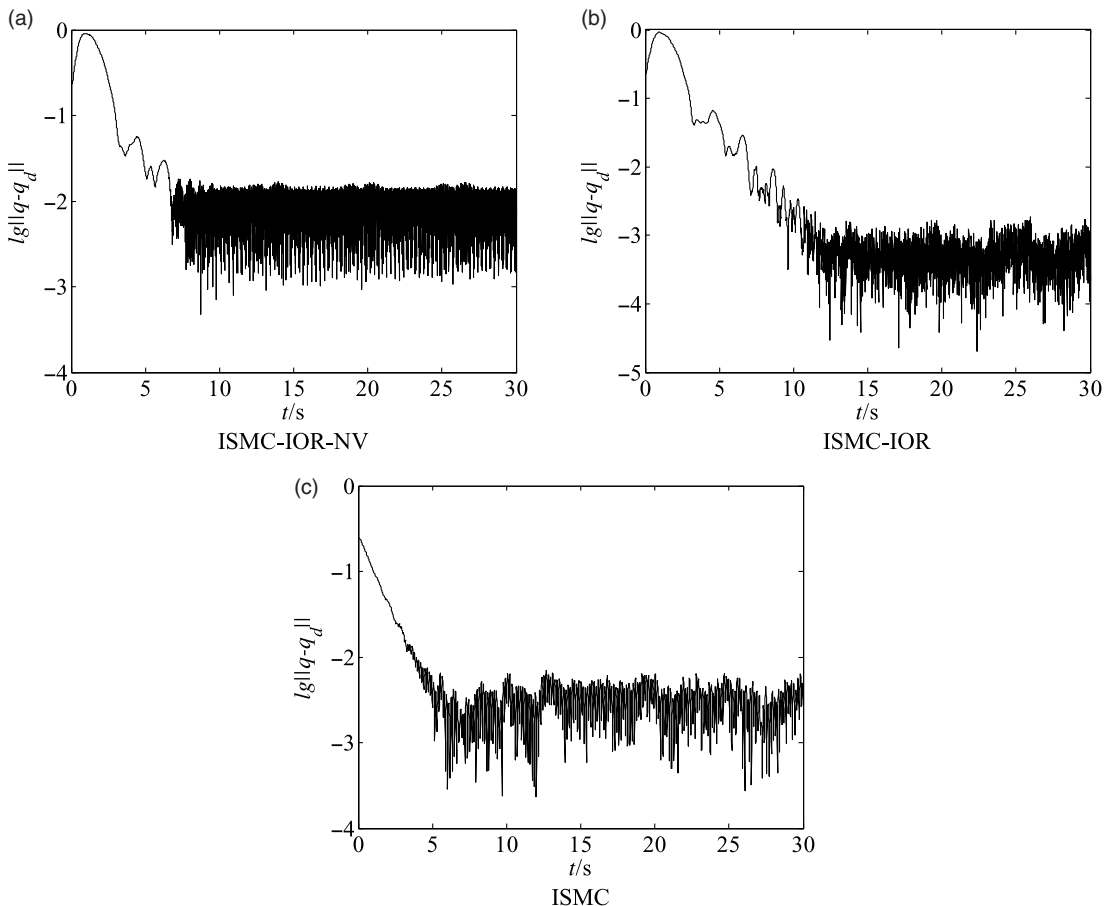
Figure 7. *Tracking error convergence rate of the FBFLFJ space robot under three control conditions. (a) ISMC-IOR-NV. (b) ISMC-IOR. (c) ISMC.*

which is maintained at 0.1 rad after stabilization. Both of them are significantly suppressed compared to the ISMC-IOR-NV control. It shows that the flexible vibration suppressor proposed in this paper can effectively suppress the flexible vibration of the base and joints.

In order to analyze the vibration of the flexible links of the FBFLFJ space robot under the two control algorithms, the following simulations are performed. Among them, Fig. 10 shows the first two orders of modal vibration curves of the link B_1 under two control conditions, and Fig. 11 shows the first two orders of modal vibration curves of the link B_2 under two control conditions.

From Figs. 10(a) and 11(a), it can be seen that under ISMC-IOR-NV control, the 1st order modal coordinates of link B_1 are maintained at 0.002 m at 20–30 s, and 0.001 m at 20–30 s for the 2nd order modal coordinates; the 1st order modal coordinates of link B_2 are maintained at 0.012 m, and 0.017 m for the 2nd order modal coordinates. As shown in Figs. 10(b) and 11(b), under ISMC-IOR control, both the 1st and 2nd order modal coordinates of the link B_1 are suppressed to within 0.001 m; the 1st order
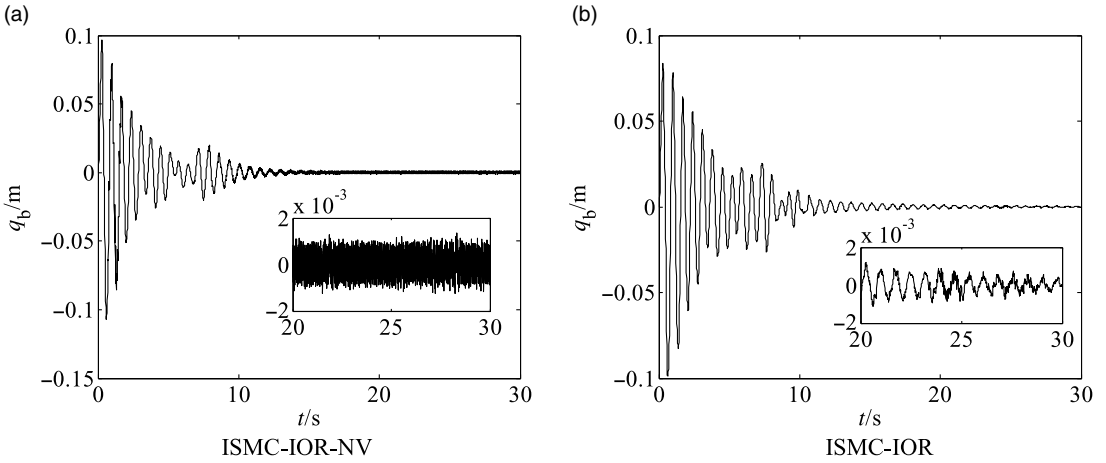
Figure 8. *Flexible vibration curve of FBFLFJ space robot base under two control conditions. (a) ISMC-IOR-NV. (b) ISMC-IOR.*
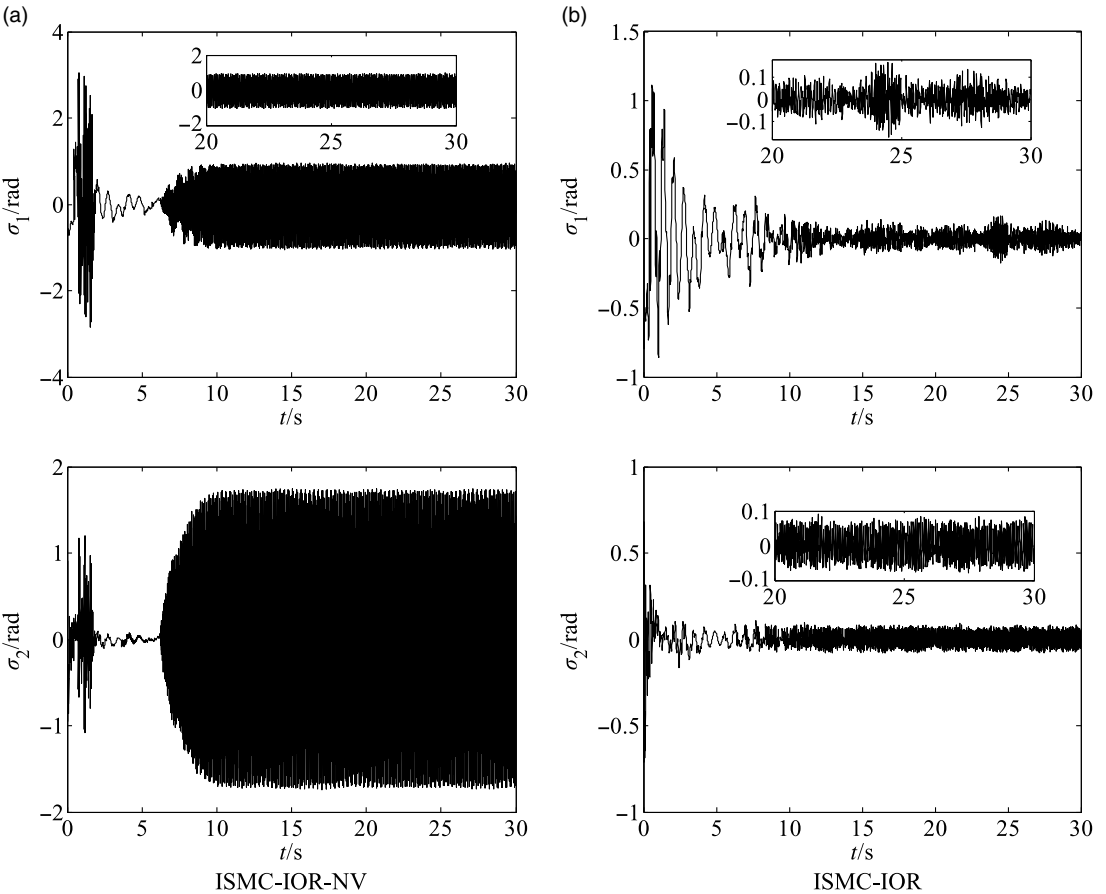

Figure 9. *Flexible vibration curve of FBFLFJ space robot joints under two control conditions. (a) ISMC-IOR-NV. (b) ISMC-IOR.*
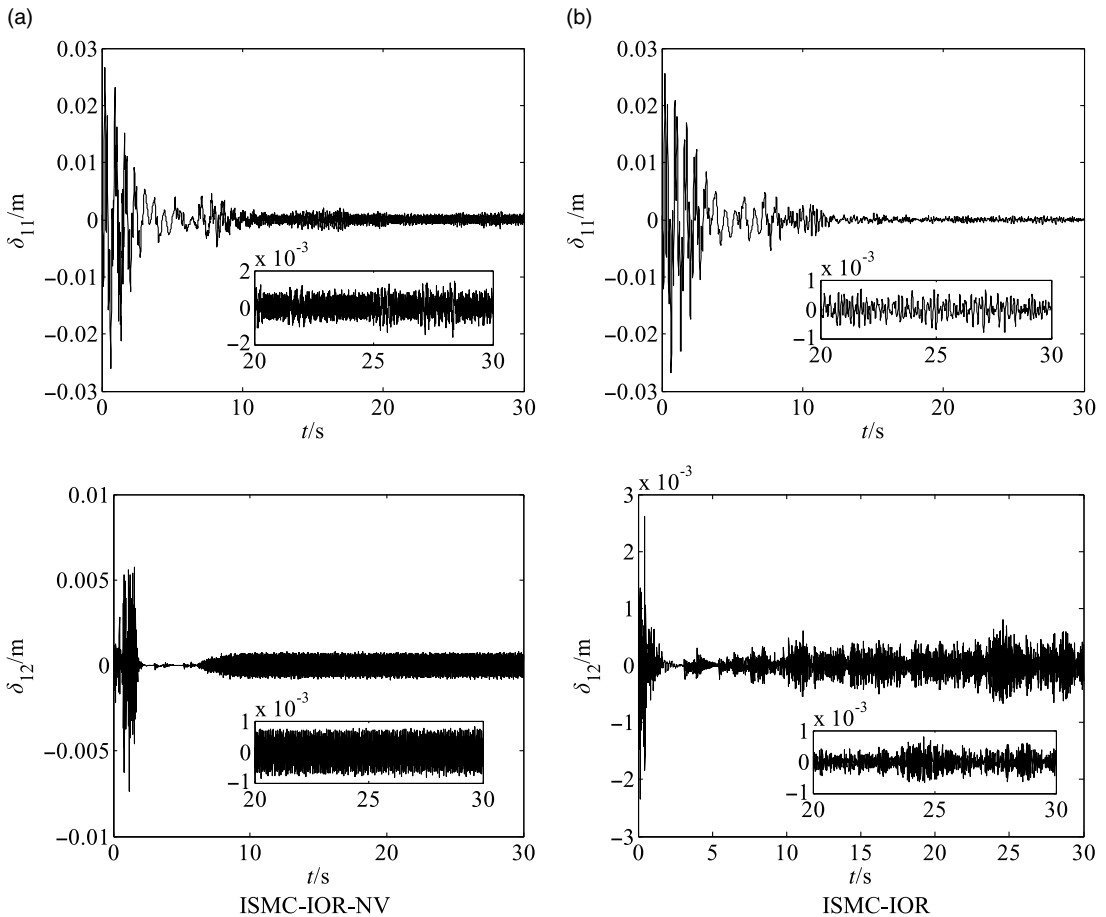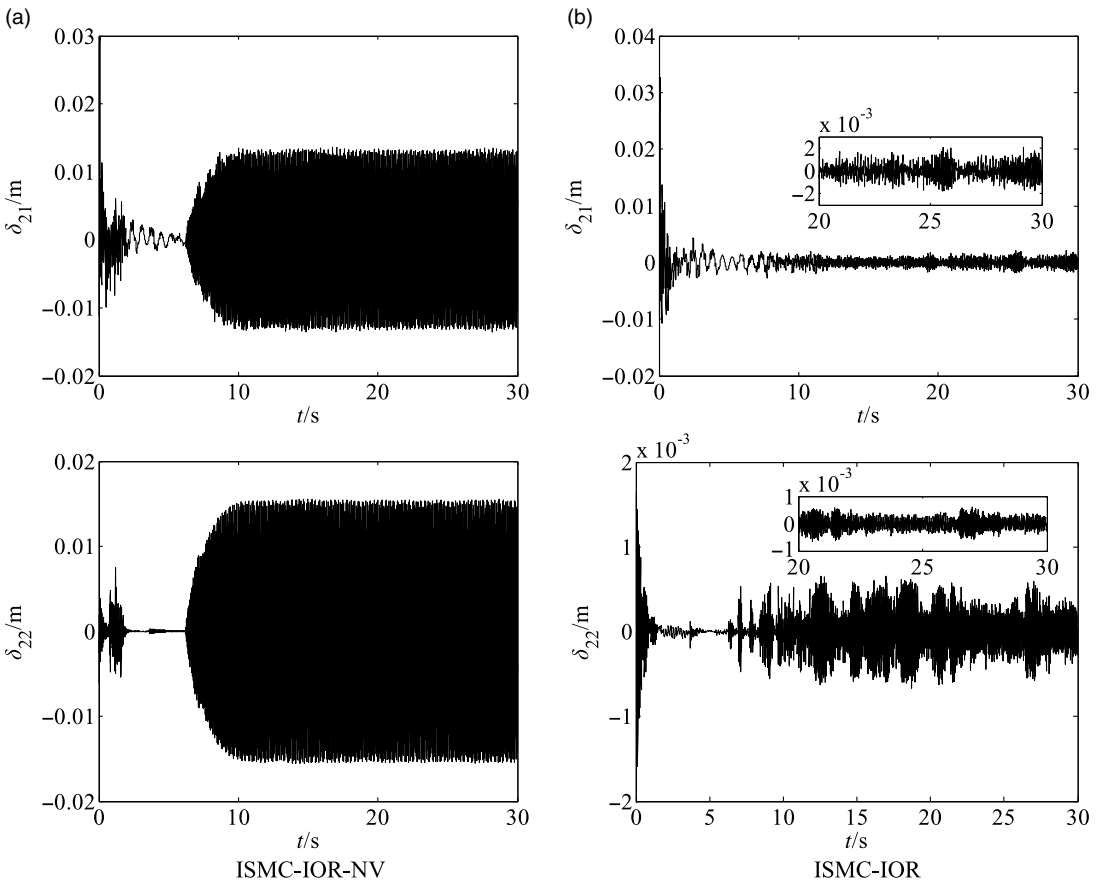
Figure 10. *Flexible vibration curve of FBFLFJ space robot link B₁ under two control conditions. (a) ISMC-IOR-NV. (b) ISMC-IOR.*

modal coordinates of the link B_2 are suppressed to 0.0025 m and the 2nd order modal coordinates are suppressed to 0.001 m. Compared with the ISMC-IOR-NV control, the modal vibration of both links under ISMC-IOR control is effectively suppressed.

In order to quantitatively analyze the suppression effect of the controller proposed in this paper on the flexible vibration of the system, the vibration of all the flexible variables of the system with the flexible suppressor on and off is analyzed in combination with Figs. 10 and 11, as shown in Table II.

As can be seen in Table II, the ISMC-IOR proposed in this paper has the obvious function of suppressing the multiple flexible vibrations of the system. Compared with ISMC-IOR-NV, the vibration suppression performance of the base, joints and links of the FBFLFJ space robot controlled by ISMC-IOR can be improved by 50%, 85%, 94.44%, 44.44%, 37.50%, 80.77% and 94.12%, respectively.

In order to verify the torque limitation of the proposed algorithm, the driving torque required for ISMC-IOR control is analyzed and the simulation results are shown in Fig. 12. It can be seen that the maximum upper bound of the real-time moment is $(\boldsymbol{\tau}_{oj})_r = \begin{bmatrix} 50 & 60 & 40 \end{bmatrix}^T$. According to $K_{0ii} + k' + 2 + \beta_i \leq (\tau_{oj,i,\max})_r$, it is obtained that $(\tau_{oj,0,\max})_r \geq 62$, $(\tau_{oj,1,\max})_r \geq 62.5$, $(\tau_{oj,2,\max})_r \geq 62.9$. The moment in the simulation satisfies the constrained relation $(\tau_{oj,i})_r \leq (\tau_{oj,i,\max})_r$, where $(\tau_{oj,i})_r$ is the element corresponding to vector $(\boldsymbol{\tau}_{oj})_r$, $i = 1, 2, 3$, so the moment constraint requirement is satisfied.

Table II.   *Vibrations of the FBFLFJ space robot base, joints and links at 20–30 s.*

No.	Flexible variables	ISMC-IOR-NV	ISMC-IOR	Performance improvement of ISMC-IOR over ISMC-IOR-NV
1	q_b/m	1.0×10^{-3}	0.5×10^{-3}	50.00%
2	σ_1/rad	1.000	0.150	85.00%
3	σ_2/rad	1.800	0.100	94.44%
4	δ_{11}/m	1.8×10^{-3}	1.0×10^{-3}	44.44%
5	δ_{12}/m	0.8×10^{-3}	0.5×10^{-3}	37.50%
6	δ_{21}/m	0.013	2.5×10^{-3}	80.77%
7	δ_{22}/m	0.017	1.0×10^{-3}	94.12%

Figure 11.   *Flexible vibration curve of FBFLFJ space robot link B$_2$ under two control conditions. (a) ISMC-IOR-NV. (b) ISMC-IOR.*

6. Conclusions

(1) For the actuator saturated space robot affected by multiple flexible vibrations of base, links and joints, the modeling method of dynamic model of FBFLFJ space robot is analyzed. On this basis, a singular perturbation decomposition scheme of the model is proposed. Then, according to the rigid flexible subsystem, we propose an algorithm of integrated sliding mode control with input restriction, output feedback and repetitive learning.
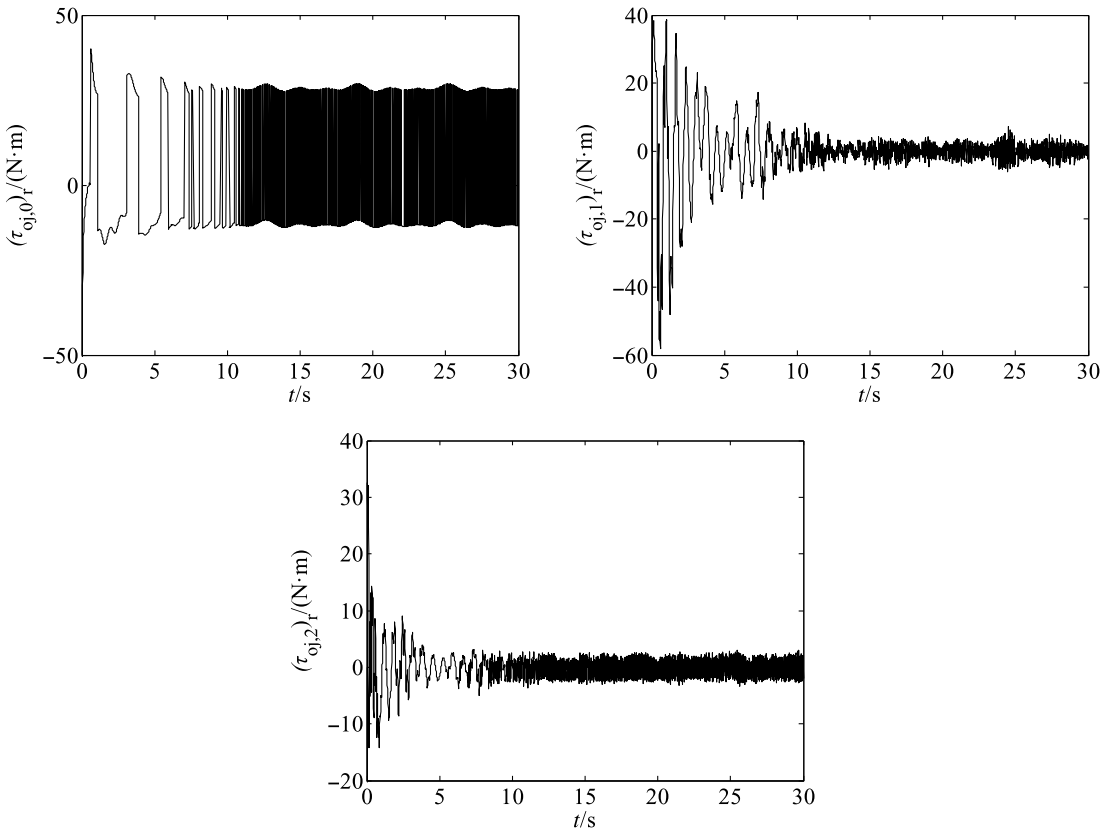
Figure 12. *Torques under ISMC-IOR.*

(2) The simulation results show that the flexible vibration significantly affects the control accuracy of the system, and the rigid controller without suppressing the flexible vibration cannot control the FBFLFJ space robot system to perform the accurate tracking task. In contrast, the controller proposed in this paper can make the system track the desired trajectory with -3 orders of magnitude accuracy while suppressing the multiple flexible vibrations of the system base, links and joints 50%–80% and 37% performance improvement were achieved. The control algorithm enables the space robot system to work with limited input torque and can also deal with the lack of model information and speed information.

Ethical considerations. None.

References

[1] R. Doyle, T. Kubota, M. Picard, B. Sommer, H. Ueno, G. Visentin and R. Volpe, "Recent research and development activities on space robotics and AI," *Adv. Robot.* **35**(21), 1244–1264 (2021).

[2] H. Q. Li, X. F. Liu, S. J. Guo and G. P. Cai, "Deployment dynamics of large-scale flexible solar arrays," *Proc. Inst. Mech. Eng. K J. Multi Body Dyn.* **230**(2), 147–158 (2016).

[3] B. Wie, A. Hu and R. Singh, "Multibody interaction effects on space station attitude-control and momentum management," *J. Guid. Control Dyn.* **13**(6), 993–999 (1990).

[4] A. M. Giordano, D. Calzolari, M. De Stefano, H. Mishra, C. Ott and A. Albu-Schäffer, "Compliant floating-base control of space robots," *IEEE Robot. Autom. Lett.* **6**(4), 7485–7492 (2021).

[5] H. P. Ai, A. Zhu and L. Chen, "Buffer compliance control of space robots capturing a non-cooperative spacecraft based on reinforcement learning," *Appl. Sci. (Switzerland)* **11**(5), 5783 (2021).

[6] S. N. Singh and A. A. Schy, "Robust Torque Control of an Elastic Robotic Arm Based on Invertibility and Feedback Stabilization," **In:** *Proceedings of the 24th IEEE Conference on Decision and Control (Cat. No.85CH2245-9)*, vol. 2 (1985) pp. 1317–1322.

[7] L. X. Liu, W. Yao and Y. Guo, "Prescribed performance tracking control of a free-flying flexible-joint space robot with disturbances under input saturation," *J. Franklin Inst.* **358**(9), 4571–4601 (2021).

[8] X. X. Yang, S. S. Ge and J. K. Liu, "Dynamics and noncollocated model-free position control for a space robot with multi-link flexible manipulators," *Asian J. Control* **21**(2), 714–724 (2019).

[9] Y. Hu, S. Y. Dian, R. Guo, S. C. Li and T. Zhao, "Observer-based dynamic surface control for flexible-joint manipulator system with input saturation and unknown disturbance using type-2 fuzzy neural network," *Neurocomputing* **436**(2), 162–173 (2021).

[10] M. A. Bégin, R. Poon and H. Ian, "Streamlined tuning procedure for stable PID control of flexible-base manipulators," *IEEE Robot. Autom. Lett.* **6**(4), 7413–7420 (2021).

[11] F. Beck, G. Garofalo and C. Ott, "Vibration Control for Manipulators on a Translationally Flexible Base," **In:** *Proceedings-IEEE International Conference on Robotics and Automation* (2019) pp. 4451–4457.

[12] R. Mori and T. Murakami, "A Fusion Control of Impedance and Vibration Suppression for a Manipulator with Flexible Base," **In:** *Proceedings of the IEEE International Conference on Industrial Technology* (2019) pp. 42–47.

[13] X. Y. Yu, "Hybrid-trajectory based terminal sliding mode control of a flexible space manipulator with an elastic base," *Robotica* **38**(3), 550–563 (2020).

[14] M. H. Korayem, S. F. Dehkordi and O. Mehrjooee, "Nonlinear analysis of open-chain flexible manipulator with time-dependent structure," *Adv. Space Res.* **69**(2), 1027–1049 (2022).

[15] M. H. Korayem, S. F. Dehkordi, M. Mojarradi and P. Monfared1, "Analytical and experimental investigation of the dynamic behavior of a revolute-prismatic manipulator with N flexible links and hubs," *Int. J. Adv. Manuf. Technol.* **103**(5-8), 2235–2256 (2019).

[16] M. Aghajari, S. F. Dehkordi and M. H. Korayem, "Nonlinear dynamic analysis of the extended telescopic joints manipulator with flexible links," *Arab. J. Sci. Eng.* **46**(8), 7909–7928 (2021).

[17] Q. Zhang, X. F. Liu and G. P. Cai, "Dynamics and control of a flexible-link flexible-joint space robot with joint friction," *Int. J. Aeronaut. Space Sci.* **22**(2), 415–432 (2021).

[18] L. M. Xie, X. Y. Yu and L. Chen, "Robust fuzzy sliding mode control and vibration suppression of free-floating flexible-link and flexible-joints space manipulator with external interference and uncertain parameter," *Robotica* **40**(4), 997–1019 (2021).

[19] T. Sands, "Flattening the curve of flexible space robotics," *Appl. Sci. Basel* **12**(6), 1–36 (2022).

[20] T. Sands, "Optimization provenance of whiplash compensation for flexible space robotics," *Aerospace* **6**(9), 1–18 (2019).

[21] S. Y. Jia and J. J. Shan, "Finite-time trajectory tracking control of space manipulator under actuator saturation," *IEEE Trans. Ind. Electron.* **67**(3), 2086–2096 (2020).

[22] L. I. Q., J. P. Yuan and C. Sun, "Robust fault-tolerant saturated control for spacecraft proximity operations with actuator saturation and faults," *Adv. Space Res.* **63**(5), 1541–1553 (2019).

[23] I. Mizumoto, S. Fujii and H. Mita, "Output feedback-based output tracking control with adaptive output predictive feedforward for multiple-input-multiple-output systems," *Ind. Eng. Chem. Res.* **58**(26), 11382–11391 (2019).

[24] Q. Z. Yan, J. P. Cai, Z. F. Li and Q. Y. Yang, "Multi-period repetitive control for nonparametric uncertain systems," *IEEE Access* **7**, 147849–147856 (2019). doi: 10.1109/ACCESS.2019.2946103.

[25] G. Fedele, "A fractional-order repetitive controller for periodic disturbance rejection," *IEEE Trans. Autom. Control* **63**(5), 1426–1433 (2018).

[26] Y. Liu, F. Guo, X. Y. He and Q. Hui, "Boundary control for an axially moving system with input restriction based on disturbance observers," *IEEE Trans. Syst. Man Cybern. Syst.* **49**(11), 2242–2253 (2019).

[27] D. W. Zhang and G. P. Liu, "Coordinated control of quasilinear multiagent systems via output feedback predictive control," *ISA Trans.* **128**(Pt A), 58–70 (2021).

[28] F. Califano, M. Bin, A. Macchelli and C. Melchiorri, "Stability analysis of nonlinear repetitive control schemes," *IEEE Control Syst. Lett.* **2**(4), 773–778 (2018).

[29] M. Spong, "Modeling and control of elastic joint robots," *J. Dyn. Syst. Meas. Control* **109**(4), 310–319 (1987).

[30] R. Kelly, V. Santibanez and A. Loria, *Control of Robot Manipulators in Joint Space* (Springer, London, 2005).

[31] H. K. Khalil, *Nonlinear Systems* (Publishing House of Electronics Industry, Upper Saddle River, 2007).

Appendix A: Proof of Lemma 1

Proof. Define the intermediate variable $s = \mathbf{Tanh}(e) + \alpha e_f$, then $\eta = s + \dot{s}$. Substitute η into Eq. (42) and take the integral to obtain

$$\int_0^t L_n(\tau)\,d\tau \le \int_0^t |s(\tau)|^T \left(\left| f_n(\tau) \right| + \left| \frac{d\big(f_n(\tau)\big)}{d\tau} \right| - K_{0ii} \right) d\tau$$

$$+ \sum_{i=1}^n |s_i(t)|\, (|f_{ni}(t)| - K_{0ii}) + \sum_{i=1}^n K_{0ii}|s_i(0)| - s^T(0) f_n(0) \tag{59}$$

$|\mathfrak{R}|$ represents a new expression after taking the absolute value of each element of vector or matrix $\mathfrak{R}$. According to $K_{0ii} > \left\| f_n(t) \right\|_\infty + \left\| \dot{f}_n(t) \right\|_\infty$ and $e_f(0) = \mathbf{0}$, Eq. (59) satisfies $\int_0^t L_n(\tau)\,d\tau \le \xi_n$. Proof complete. $\square$

Appendix B: Proof of Theorem 1

Proof. Case I. $\left| \big(Q_0 z_0 + \sum_{k=1}^N Q_k \dot{z}_k \big)_i \right| > \beta_i$ for all i.

Define auxiliary function $P_1(t) = \xi_1 - \int_0^t L_1(\tau)\,d\tau$ and variable $\int_0^{v_i} \tanh \tau \operatorname{sech}^2 \tau\,d\tau$. $P_1(t) \ge 0$ is obtained from Lemma 1 and Eq. (45), in combination with $\int_0^{v_i} \tanh \tau \operatorname{sech}^2 \tau\,d\tau \ge 0$, the Lyapunov function V_1 is constructed as

$$V_1 = \sum_{i=1}^3 \ln(\cosh e_i) + \sum_{i=1}^3 \int_0^{v_i} \tanh \tau \operatorname{sech}^2 \tau\,d\tau + \frac{1}{2} e_f^T e_f + \frac{1}{2} \eta^T M(\delta, q)\, \eta + P_1 = y_1^T U_1 y_1, \tag{60}$$

where $y_1 = \left[Ln^T(e)\ \ Fn^T(v)\ \ e_f^T\ \ \eta^T\ \ \sqrt{P_1} \right]^T$, $Ln(e) = \left[\sqrt{\ln(\cosh e_1)}\ \ \sqrt{\ln(\cosh e_2)}\ \ \sqrt{\ln(\cosh e_3)} \right]^T$, and $Fn(v) = \left[\sqrt{\int_0^{v_1} \tanh \tau \operatorname{sech}^2 \tau\,d\tau}\ \ \ \sqrt{\int_0^{v_2} \tanh \tau \operatorname{sech}^2 \tau\,d\tau}\ \ \ \sqrt{\int_0^{v_3} \tanh \tau \operatorname{sech}^2 \tau\,d\tau} \right]^T$. $\square$

According to the value of stability condition $\lambda_{11}, \lambda_{12}$ and Eq. (60), we get

$$\lambda_{11} \left\| y_1 \right\|^2 \le V_1\big(t, y_1\big) \le \lambda_{12} \left\| y_1 \right\|^2. \tag{61}$$

Derive from Eq. (60), and according to Eqs. (33)–(39), we have

$$\dot{V}_1 = \dot{V}_H + \dot{P}_1 + \eta^T \cdot \left[N_d - B \cdot \mathbf{Sgn}\left(Q_0 z_0 + \sum_{k=1}^N Q_k \dot{z}_k \right) - K_0 \mathrm{sgn}\big(\mathbf{Tanh}(e) + \alpha e_f\big) \right], \tag{62}$$

$$\dot{V}_H = -\mathbf{Tanh}^T(e)\,\mathbf{Tanh}(e) - \mathbf{Tanh}^T(v) \cdot \mathbf{Tanh}(v) + \alpha^{-1} e_f^T \big(I_3 - \mathbf{Sech}^2(e)\big)\,(\eta - \mathbf{Tanh}(e) - \mathbf{Tanh}(v))$$

$$- e_f^T e_f + \eta^T \tilde{N} - k' \eta^T M(\delta, q)\, \eta - \eta^T M(\delta, q)\,\big(I_3 - \mathbf{Sech}^2(e)\big)\,\eta. \tag{63}$$

Substitute $f_1(t)$ and $P_1(t) = \xi_1 - \int_0^t L_1(\tau)\,d\tau$ into Eq. (62) to get $\dot{V}_1 = \dot{V}_H$. By substituting Eqs. (41), (46) and (47) into $\dot{V}_H$, and according to λ_3, we have

$$\dot{V}_H \le -\lambda_3 \left\| \mathbf{Tanh}(e) \right\|^2 - \lambda_3 \left\| \mathbf{Tanh}(v) \right\|^2 - \lambda_3 \left\| e_f \right\|^2 - \lambda_3 \left\| \eta \right\|^2 + \rho^2(\|z\|)\, \|z\|^2 / (4k_n) = -\gamma \left\| z \right\|^2, \tag{64}$$

where $\gamma = \lambda_3 - \dfrac{\rho^2(\|z\|)}{4k_n}$. According to the stability condition Eq. (48), it can be seen that $\gamma \|z\|^2$ is a continuous positive semidefinite function on the attraction domain $\boldsymbol{D} = \left\{ \boldsymbol{y}_1 \mid \|z\| < \rho^{-1}\left(2\sqrt{\lambda_3 k_n}\right) \right\}$, and that there exists a domain of attraction $S_1 \subset \boldsymbol{D}$ as

$$ S_1 = \left\{ \boldsymbol{y}_1 \in \boldsymbol{D} \mid \lambda_{12} \left\| \boldsymbol{y}_1 \right\|^2 < \lambda_{12}\left[\rho^{-1}\left(2\sqrt{\lambda_3 k_n}\right)\right] \right\}. \tag{65} $$

According to the invariance-like theorem which is detailed in theorem 8.4 by Khalil [31], it can be seen that $\forall \boldsymbol{y}_1(0) \in S_1$. When, $t \to \infty$, $\gamma \|z\|^2 \to 0$. Combined with the definition of vector z and the expression of vector $\boldsymbol{\eta}$ in Eq. (41), it can be seen that when $t \to \infty$, $\boldsymbol{e}(t), \boldsymbol{e}_f(t), \boldsymbol{v}(t), \boldsymbol{\eta}(t), \dot{\boldsymbol{e}}(t) \to 0$.

Case II. $\left| \left(\boldsymbol{Q}_0 z_0 + \sum_{k=1}^{N} \boldsymbol{Q}_k \dot{z}_k\right)_i \right| \le \beta_i$ for all i.
Introduce variable $\tilde{z}_k = z_k - z_k^* \ (k = 1, \cdots N)$, let

$$ \begin{cases} z_0^* = \boldsymbol{Q}_0^{-1} \overline{a}_0 \\ z_k^* = (k\omega)^{-1} \boldsymbol{Q}_k^{-1} \left[\overline{a}_k \sin(k\omega t) - \overline{b}_k \cos(k\omega t) \right] \end{cases}. \tag{66} $$

Since $\ddot{z}_k^* = -(k\omega)^2 z_k^*$, the closed-loop system variables are as follows:

$$ \begin{cases} \dot{\tilde{z}}_0 = \boldsymbol{Q}_0 \boldsymbol{\eta} \\ \ddot{\tilde{z}}_k + k^2\omega^2 \tilde{z}_k = \boldsymbol{Q}_k \boldsymbol{\eta} \qquad (k = 1, \cdots N) \end{cases}. \tag{67} $$

Construct the Lyapunov function V_2 as

$$ V_2 = \sum_{i=1}^{3} \ln(\cosh e_i) + \sum_{i=1}^{3} \int_0^{v_i} \tanh \tau \ \mathrm{sech}^2 \tau \mathrm{d}\tau + \frac{1}{2}\boldsymbol{e}_f^T \boldsymbol{e}_f + \frac{1}{2}\boldsymbol{\eta}^T \boldsymbol{M}(\boldsymbol{\delta}, \boldsymbol{q})\, \boldsymbol{\eta} + P_2 $$

$$ + \frac{1}{2}\tilde{z}_0^T \boldsymbol{Q}_0 \tilde{z}_0 + \frac{1}{2}\sum_{k=1}^{N} \dot{\tilde{z}}_k^T \dot{\tilde{z}}_k + \frac{1}{2}\sum_{k=1}^{N} k^2\omega^2 \tilde{z}_k^T \tilde{z}_k = \boldsymbol{y}_2^T \boldsymbol{U}_2 \boldsymbol{y}_2, \tag{68} $$

where $\boldsymbol{y}_2 = \begin{bmatrix} \boldsymbol{Ln}^T(\boldsymbol{e}) & \boldsymbol{Fn}^T(\boldsymbol{v}) & \boldsymbol{e}_f^T & \boldsymbol{\eta}^T & \sqrt{P_2} & \tilde{z}_0^T & \tilde{z}_1^T & \cdots & \tilde{z}_N^T & \dot{\tilde{z}}_1^T & \cdots & \dot{\tilde{z}}_N^T \end{bmatrix}^{\mathrm{T}}$. According to the value of stability condition λ_{21} and λ_{22}, combined with Eq. (68) we have

$$ \lambda_{21} \left\| \boldsymbol{y}_2 \right\|^2 \le V_2(t, \boldsymbol{y}_2) \le \lambda_{22} \left\| \boldsymbol{y}_2 \right\|^2. \tag{69} $$

Take the derivative of Eq. (68), substitute the right side of the resulting equation into Eqs. (34), (35), (39) and (67), and according to $\boldsymbol{f}_2(t)$ and $P_2(t) = \xi_2 - \int_0^t L_2(\tau) \, \mathrm{d}\tau$, we have

$$ \dot{V}_2 = \mathbf{Tanh}^T(\boldsymbol{e}) \cdot \dot{\boldsymbol{e}} + \mathbf{Tanh}^T(\boldsymbol{v}) \ \mathbf{Sech}^2(\boldsymbol{v}) \ \dot{\boldsymbol{v}} + \boldsymbol{e}_f^T \dot{\boldsymbol{e}}_f + \frac{1}{2}\boldsymbol{\eta}^T \dot{\boldsymbol{M}}(\boldsymbol{\delta}, \boldsymbol{q})\, \boldsymbol{\eta} $$

$$ + \boldsymbol{\eta}^T \boldsymbol{M}(\boldsymbol{\delta}, \boldsymbol{q})\, \dot{\boldsymbol{\eta}} + \dot{P}_2 + \tilde{z}_0^T \dot{\tilde{z}}_0 + \sum_{k=1}^{N} \dot{\tilde{z}}_k^T \ddot{\tilde{z}}_k + \sum_{k=1}^{N} k^2\omega^2 \tilde{z}_k^T \dot{\tilde{z}}_k = \dot{V}_H. \tag{70} $$

According to Eqs. (63) and (64), we get $\dot{V}_H \le -\gamma \|z\|^2$, and its continuous semi-positive definite on the domain of attraction $\boldsymbol{D}$, according to the stability condition Eq. (48), we get the domain of attraction $S_2 \subset \boldsymbol{D}$ as

$$ S_2 = \left\{ \boldsymbol{y}_2 \in \boldsymbol{D} \mid \lambda_{22} \left\| \boldsymbol{y}_2 \right\|^2 < \lambda_{22} \left[\rho^{-1}\left(2\sqrt{\lambda_3 k_n}\right)\right] \right\}. \tag{71} $$

Based on the invariance-like theorem, $\forall \boldsymbol{y}_2(0) \in S_2$. When $t \to \infty$, $\boldsymbol{e}(t), \boldsymbol{e}_\mathrm{f}(t), \boldsymbol{v}(t), \boldsymbol{\eta}(t), \dot{\boldsymbol{e}}(t) \to 0$. Proof complete.

Appendix C: Acronyms description, as shown in Table III.

Table III. *Acronyms description.*

Acronym	Notes
FBFLFJ	Flexible-base flexible-links flexible-joints
SMC	Sliding mode control
SMC-IOR	Sliding mode control with input restriction, output feedback and repetitive learning
SMC-IOR-D	Sliding mode control with input restriction, output feedback and repetitive learning based on the desired trajectory
SMC-IOR-H	Sliding mode control with input restriction, output feedback and repetitive learning based on hybrid trajectory
ISMC	Integrated sliding mode control for motion and vibration algorithm without repetitive learning controller
ISMC-IOR	Integrated sliding mode control with input restriction, output feedback and repetitive learning
ISMC-IOR-NV	Integrated sliding mode control with input restriction, output feedback and repetitive learning without vibration suppression